the remnant infectivity in the treated samples. In addition, a protein misfolding cyclic amplification (PMCA), which is a highly sensitive method for detecting minute amounts of PrP^{Sc} [17,18], was employed for the detection of residual PrP^{Sc} following the Maillard reaction.

Materials and methods

Maillard reaction. The hamster-adapted scrapie prion strain Sc237 was propagated in hamsters. The brains of hamsters in the terminal stage of the disease, titrating $5 \times 10^{8.5}$ lethal dose (LD_{50}) per gram by bioassay [19], were pooled and homogenized at a concentration of 20% (w/v) in PBS. The homogenate (250 μl) was mixed with an equal volume of 0%, 10%, 20% or 40% (w/v) of glucose–PBS solution in the presence of 2% (w/v) sodium hydrogen carbonate. Since the kinetics of the Maillard reaction depend upon the pH and temperature conditions and the maximum reaction velocity can be obtained in pH ranges of 9–10 [20–22], sodium hydrogen carbonate was added to the reaction buffer as a pH-controlling reagent. After incubation for 30 min at room temperature, the samples were heated to 100 °C and kept for 3 h. After the above treatment, the samples were cooled down to the ambient temperature and the resultant materials were stored at −80 °C until further use.

Western blotting and sequential PMCA. The samples treated by the Maillard reaction and a control sample were mixed with an equal volume of 2× SDS sample buffer and incubated at 100 °C for 5 min. The samples were separated by SDS–PAGE and transferred onto a polyvinylidene fluoride membrane (Millipore, Bedford, MA). After blocking, the membrane was incubated for 1 h with horseradish peroxidase-conjugated 3F4 (1/2500; Signet Laboratories, Dedham, MA) or SAF32 (1/2500; Cayman chemical, Ann Arbor, MI) monoclonal antibodies. After washing, the blotted membrane was developed with the ECL + Plus Western Blotting Detection System (Amersham Biosciences, Buckinghamshire, England) according to the manufacturer's instructions. The chemiluminescence signals were analyzed using the Light Capture System (ATTO, Tokyo, Japan).

We used the PMCA procedure described in our previous study [19]. Briefly, normal hamster brains were homogenized at 10% (w/v) in PBS-containing complete protease inhibitors (Roche Diagnostics, Mannheim, Germany), 1% Triton X-100, and 4 mM EDTA. The supernatant was separated by brief centrifugation and used as the PrP^{C} source. The sample was diluted 1:10 in normal brain homogenate, and one round of the PMCA reaction was carried out by performing 40 cycles of sonication followed by incubation at 37 °C for 1 h. Next, the process of dilution (1:10) of the PMCA product and its subsequent amplification was repeated two times. In the case of PMCA products, before and after each round of amplification, samples (10 μl) were mixed with 10 μl of proteinase K (PK) solution (100 μg/ml) and incubated at 37 °C for 1 h. The digested materials were analyzed by Western blotting using the 3F4 antibody as described above.

Bioassay. The inactivated samples were ultrasonicated immediately before inoculation. In the preliminary experiments, convulsions developed in the mice inoculated with the samples containing 5% or 10% glucose at final concentration, and some mice died within 15 min. Therefore, the samples with 20% glucose at final concentration and those without glucose (temperature control) were injected intracerebrally into five or six Tg52NSE mice (20 μl per mouse) that exhibited over expression of hamster PrP^{C} in their nerve system [23]. All animal experiments were performed according to the guidelines of the National Institute of Animal Health.

Results

Characterization of PrP^{Sc} after the Maillard reaction

Fig. 1 illustrates the results of Western blotting following the Maillard reaction. The signal intensities of both

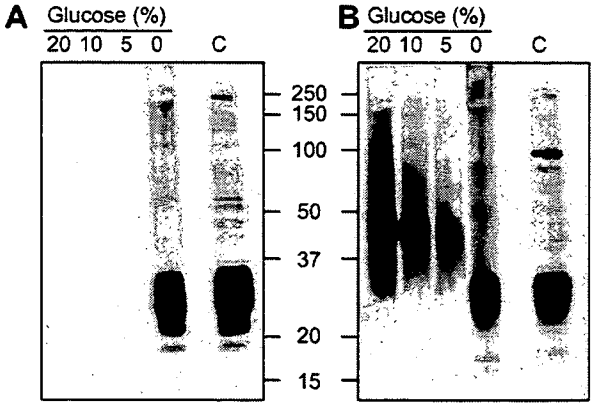

Fig. 1. Western blot analysis of prion protein in the Sc237-infected hamster brain homogenate following the Maillard reaction. A 20% brain homogenate and 0–40% of the glucose solution were mixed in equal quantities: the mixture was then incubated at 100 °C for 3 h in the presence of 2% sodium hydrogen carbonate. The samples were separated by SDS–PAGE, and the blotted membranes were then incubated with 3F4 (A) or SAF32 (B) antibodies. The lanes labeled "C" were the controls in which no glucose was added to the mixture before heating. The positions of molecular-weight standards (15–250 kDa) are also shown.

3F4 (A) and SAF32 (B) epitopes of prion protein did not differ greatly in the samples before (lane "C") and after heating in the presence of sodium hydrogen carbonate alone. The 3F4 epitope (MKHM) could no longer be detected following the Maillard reaction in the presence of 5–20% of glucose. The chemical modification of the lysine residue located in the epitope by glucose is probably responsible for this observation. On the other hand, the SAF32 epitope within the octapeptide repeat region (WGQPHGGG) could be detected as broad signals following the Maillard reaction. The epitope did not consist of reactive amino acid residues; therefore, the antigenicity was maintained after the Maillard reaction. The molecular weight of the prion protein detected by the SAF32 antibody was significantly increased, indicating that the addition of glucose to the reactive amino acid residues located outside of the epitope proceeded to various extents during the reaction. These results suggested that the molecular structure of prion protein was considerably altered by the Maillard reaction.

Assessment by the bioassay and PMCA

The control mice inoculated with the untreated samples developed the disease after an average period of 45 ± 2 days (average ± SD, $n = 5$, Fig. 2). The mice inoculated with the heat-treated (100 °C for 3 h) control sample died after an average period of 49 ± 2 days ($n = 5$). The onset of the disease in the mice inoculated with the sample containing 20% glucose at final concentration treated by the Maillard reaction was significantly delayed; however, they died after an average period of 115 ± 30 days ($n = 6$). The reduction in infectivity was estimated to be

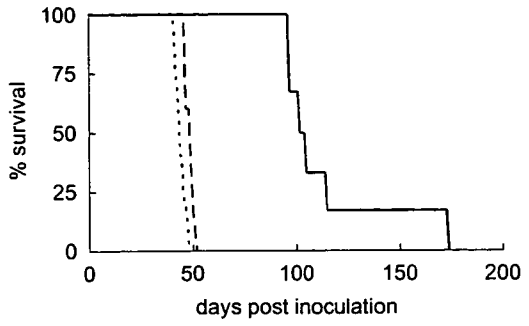

Fig. 2. Survival curves of Tg52NSE mice inoculated with the infected brain homogenates. Dotted line, no treatment; broken line, heat treatment (100 °C, 3 h) alone; solid line, the Maillard reaction with 20% glucose at final concentration.

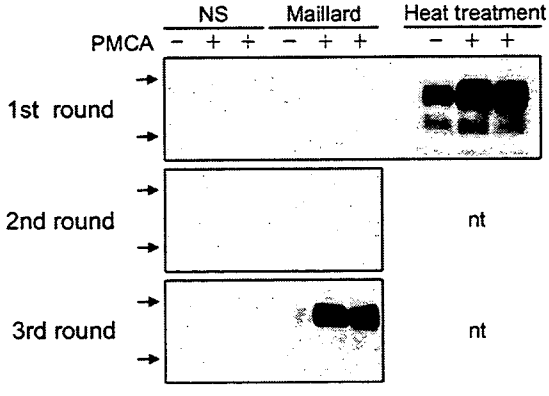

Fig. 3. PMCA of the sample containing 20% glucose at final concentration following the Maillard reaction. The sequential PMCA was performed according to the procedure described in our previous report [19]. The samples were analyzed before (−) and after (+, in duplicate) each round of amplification by Western blotting following digestion with PK. The lanes labeled "NS" were the controls in which the uninfected brain homogenate (PrP^C only) was treated in the same manner. No signals were detected in these samples. The lanes labeled "Heat treatment" denote the controls in which the infected brain homogenate was subjected to only heat treatment (100 °C, 3 h). The arrows indicate the positions of the molecular-weight markers corresponding to 30 and 20 kDa. nt, not tested.

$10^{-5.9}$ on the basis of the incubation time obtained from the previous study [19].

Fig. 3 shows the results from the amplification of the samples treated by the Maillard reaction. In the first and second rounds of amplification, no protease-resistant PrP (PrP^{res}) signals were detected in the samples. However, after three rounds of amplification, the PrP^{res} signals could be detected in both the duplicated samples. These results suggested that a minute amount of PrP^{Sc} remained unmodified in the sample treated by the Maillard reaction.

Discussion

The Maillard reaction has been considered to be the chemical reaction responsible for the browning and the loss of nutritive value of foods. The reaction involves the formation of CO_2 from the carboxyl group of the amino acid residue of proteins and the development of brown pigments (melanoidins), which might be nitrogen-containing polymeric substances of proteins. There are numerous reports describing the chemistry of this complex reaction to identify its various pathways, including reaction parameters such as pH, temperature, time, sugar reactivity, concentration of the reagents, water content, and glass transition temperature [21,22,24]. In the present study, we assessed various concentrations of glucose in the presence of sodium hydrogen carbonate for the ability to reduce infectivity and decrease PrP^{Sc} levels by the bioassay and the PMCA, respectively.

Since PrP^{Sc} is resistant against physicochemical inactivation procedures, very harsh treatments are required for complete inactivation of PrP^{Sc}. A majority of chemicals, that are strong protein-modification agents may cause secondary damage such as environmental pollution and are not suitable for MBM treatment. On the other hand, the advantages of the Maillard reaction are the low corrosive impact and chemical toxicity. The reactants are nontoxic reducible carbohydrates such as glucose; further, the products appear to be harmless because the Maillard reaction generally occurs during the manufacturing processes of heat-treated foodstuffs.

In conclusion, the present study demonstrated that the Maillard reaction induced a strong modification of PrP^{Sc} resulting in an effective reduction of the infectivity. Since PMCA was capable of amplifying unmodified PrP^{Sc} following the Maillard reaction and three rounds of PMCA required only 6 days, the PMCA technique would be very useful for further improvements in the process of prion decontamination by using the Maillard reaction. Studies are now in progress to validate glucose formulation as an effective yet routinely applicable reprocessing procedure for prion decontamination.

Acknowledgments

This study was supported by a Grant-in-Aid from the BSE Control Project of the Ministry of Agriculture, Forestry and Fisheries of Japan.

References

[1] S.B. Prusiner, Molecular biology of prion diseases, Science 252 (1991) 1515–1522.
[2] B.W. Caughey, A. Dong, K.S. Bhat, D. Ernst, S.F. Hayes, F.S. Caughey, Secondary structure analysis of the scrapie-associated protein PrP27-30 in water by infrared spectroscopy, Biochemistry 30 (1991) 7672–7680.
[3] K.M. Pan, M. Baldwin, J. Nguyen, M. Gasset, A. Serban, D. Groth, I. Mahlhorn, Z. Huang, R.J. Fletterick, F.E. Cohen, S.B. Prusiner, Conversion of α-helices into β-sheets features in the formation of the scrapie prion proteins, Proc. Natl. Acad. Sci. USA 90 (1993) 10962–10966.
[4] P. Brown, E.H. Rau, B.K. Johnson, A.E. Bacote, C.J. Gibbs, D.C. Gajdusek, New studies on the heat resistance of hamster-adapted scrapie agent: threshold survival after ashing at 600 degrees C

suggests an inorganic template of replication, Proc. Natl. Acad. Sci. USA 97 (2000) 3418–3421.
[5] D.M. Taylor, Resistance of transmissible spongiform encephalopathy agents to decontamination, in: H.F. Rabenau, J. Ciantl, H.W. Doerr (Eds.), Prions. A challenge for science, medicine and public health system, Karger, Basel, 2001, pp. 58–67.
[6] G.A. Wells, A.C. Scott, C.T. Johnson, R.F. Gunning, R.D. Hancock, M. Jeffrey, M. Dawson, R. Bradley, A novel progressive spongiform encephalopathy in cattle, Vet. Rec. 121 (1987) 419–420.
[7] J.W. Wilesmith, G.A.H. Wells, M.P. Cranwell, J.B. Ryan, Bovine spongiform encephalopathy: epidemiological studies, Vet. Rec. 123 (1988) 638–644.
[8] J.W. Wilesmith, J.B.M. Ryan, M.J. Atkinson, Bovine spongiform encephalopathy: epidemiological studies on the origin, Vet. Rec. 128 (1991) 199–203.
[9] J.W. Wilesmith, J.B.M. Ryan, W.D. Hueston, L.J. Hoinville, Bovine spongiform encephalopathy: epidemiological features 1985 to 1990, Vet. Rec. 130 (1992) 90–94.
[10] J.W. Baynes, S.R. Thorpe, M.H. Murtiashaw, Nonenzymatic glucosylation of lysine residues in albumin, Methods Enzymol. 106 (1984) 88–98.
[11] K.M. Biemel, O. Reihl, J. Conrad, M.O. Lederer, Formation pathways for lysine-arginine cross-links derived from hexoses and pentoses by Maillard processes, J. Biol. Chem. 276 (2001) 23405–23412.
[12] M. Akagawa, T. Sasaki, K. Suyama, Oxidative deamination of lysine residue in plasma protein of diabetic rats. Novel mechanism via the Maillard reaction, Eur. J. Biochem. 269 (2002) 5451–5458.
[13] S.R. Thorpe, J.W. Baynes, Maillard reaction products in tissue proteins: new products and new perspectives, Amino Acids 25 (2003) 275–281.
[14] M. Akagawa, D. Sasaki, Y. Kurota, K. Suyama, Formation of α-aminoadipic and γ-glutamic semialdehydes in proteins by the Maillard reaction, Ann. N. Y. Acad. Sci. 1043 (2005) 129–134.
[15] O. Frank, T. Hofmann, On the influence of the carbohydrate moiety on chromophore formation during food-related Maillard reaction of pentoses, hexoses, and disaccharides, Helv. Chim. Acta 83 (2000) 3246–3264.
[16] P.H. Lowy, H. Noak, Preparation of N-substituted 1-amino-1-deoxy-D-arabino-hexuloses of arginine, histidine, and lysine, J. Am. Chem. Soc. 78 (1956) 3175–3179.
[17] G.P. Saborio, B. Permanne, C. Soto, Sensitive detection of pathological prion protein by cyclic amplification of protein misfolding, Nature 411 (2001) 810–813.
[18] P. Saá, J. Castilla, C. Soto, Ultra-efficient replication of infectious prions by automated protein misfolding cyclic amplification, J. Biol. Chem. 281 (2006) 35245–35252.
[19] Y. Murayama, M. Yoshioka, H. Horii, M. Takata, T. Yokoyama, T. Sudo, K. Sato, M. Shinagawa, S. Mohri, Protein misfolding cyclic amplification as a rapid test for assessment of prion inactivation, Biochem. Biophys. Res. Commun. 348 (2006) 758–762.
[20] M. Takagi, N. Morita, Lysine-catalyzed Maillard browning of sugar-related compounds smaller than tetrose, in neutral and alkaline solution, Dev. Food Sci. 13 (1985) 49–57.
[21] C.H. Lea, R.S. Hannan, The effect of activity of water, of pH, and of temperature on the primary reaction between casein and glucose, Biochem. Biophys. Acta 3 (1949) 315–325.
[22] J.C. Underwood, H.G. Lento, C.O. Willets, Browning of sugar solutions. 3. Effects of pH on the color produced in dilute glucose solutions containing amino acid with amino group in different positions in molecule, J. Chem. Soc. 1959 (1959) 181–184.
[23] R.E. Race, S.A. Priola, R.A. Bessen, D. Ernst, J. Dockter, G.F. Rall, L. Mucke, B. Chesebro, M.B. Oldstone, Neuron-specific expression of a hamster prion protein minigene in transgenic mice induces susceptibility to hamster scrapie agent, Neuron 15 (1995) 1183–1191.
[24] P.A. Finot, Historical perspective of the Maillard reaction in food science, the Maillard reaction—chemistry at the interface of nutrition, aging and disease, Ann. N. Y. Acad. Sci. 1043 (2005) 1–8.

fluoride dentifrice. Therefore, they did receive a conventional intervention. Of interest, in a recent 12-month follow-up study of a small number of irradiated patients with head and neck cancer, the investigators found no microbiologic evidence for radiation periodontitis in contrast to caries pathogens and the risk for dental caries.[29]

Although the number of subjects in our study was small, this was not dissimilar from the number of patients reported in analogous investigations. Also, the microbiologic and clinical data in our study were more extensive than data reported previously by other authors[30] Figures 1 and 2.

REFERENCES

1. Scully C, Epstein JB. Oral health care for the cancer patient. Eur J Cancer B Oral Oncol 1996;5:281–292
2. Epstein JB, Scully C. The role of saliva in oral health and causes and effects of xerostomia. J Can Dent Assoc 1992;58:217–221
3. Silverman S Jr. Oral Cancer, 5th ed. Hamilton, Ontario: BC Decker Inc, 2003:113–128
4. Ohrn K. The role of oral sequelae in health-related quality of life of cancer patients. Support Care Cancer 2002;10:656–658
5. Khan SA, Wingard JR. Infection and mucosal injury in cancer treatment. J Natl Cancer Inst Monogr 2001;29:31–36
6. Sonis ST, Elting LS, Keefe D, et al. Perspectives on caner therapy-induced mucosal injury. Cancer 2004;100(suppl): 1995–2025
7. Szabo G. Treatment of xerostomia with pilocarpine. Based on 15 years' experience and treatment of 500 patients. Fogorv Sz 1985;78:65–69
8. Johnson JT, Ferretti GA, Nethery WJ, et al. Oral pilocarpine for post irradiation xerostomia in patients with head and neck cancer. N Engl J Med 1993;329:390–395
9. Gornitsky M, Shenouda G, Sultanem K, et al. Double-blind randomized, placebo-controlled study of pilocarpine to salvage salivary gland function during radiotherapy of patients with head and neck cancer. Oral Surg Oral Med Oral Pathol Oral Radiol Endod 2004;981:45–52
10. Antonadou D, Pepelassi M, Synodinoum M, et al. Prophylactic use of amifostine to prevent radiochemotherapy-induced mucositis and xerostomia in head-and-neck cancer. Int J Radiat Oncol Biol Phys 2002;52:739–747
11. Mansson-Rahemtulla B, Pruitt KM, Tenovuo J, et al. A mouthrinse which optimizes in vivo generation of hypothiocyanite. J Dent Res 1983;62:1062–1066
12. Lenander-Lumikari M, Mikola H, Tenovuo J. Effects of a lactoperoxidase system-containing toothpaste on levels of hypothiocyanite and bacteria in saliva. Caries Res 1993;27:285–291
13. Tenovuo J. Clinical applications of antimicrobial host proteins lactoperoxidase, lysosome and lactoferrin in xerostomia: efficacy and safety. Oral Diseases 2002;8:23–29
14. Kirstila V, Lenander-Lumikari M, Tenovuo J. Effects of a lactoperoxidase system-containing toothpaste on dental plaque and whole saliva in vivo. Acta Odontol Scand 1994;52:346–353
15. Sari K, Dombi C, Czeglédy A, et al. Treatment of xerostomia with lactoperoxidase-containing mouthwashes and toothpaste. Fogorv Sz 1994;87:263–272
16. van Steenberghe D, Van den Eynde E, Jacobs R, et al. Effect of a lactoperoxidase containing toothpaste in radiation-induced xerostomia. Int Dent J 1994;44:133–138
17. Toljanic JA, Siddiqui AA, Patterson GL, et al. An evaluation of a dentifrice containing salivary peroxidase elements for the control of gingival disease in patients with irradiated head and neck cancer. J Prosthet Dent 1996;76:292–296
18. Epstein JB, Emerton S, Le ND, et al. A double-blind crossover trial of Oral Balance gel and Biotène toothpaste versus placebo in patients with xerostomia following radiation therapy. Oral Oncol 1999;35:132–137
19. Warde P, Kroll B, O'Sullivan B, et al. A phase II study of Bioténe in the treatment of postradiation xerostomia in patients with head and neck cancer. Support Care Cancer 2000;8: 203–208
20. Mulligan R, Navazesh M, Slots J. Antibacterial activity of an alcohol free mouthwash with enzymes [Abstract]. J Dent Res 1992;71:156
21. Kielbassa AM, Shohadai SP, Shulte-Möntig J. Effect of saliva substitutes on mineral content of demineralised and sound dental enamel. Support Care Cancer 2000;9:40–47
22. Sreebny L, Zhu WX. Whole saliva and the diagnosis of Sjögren's syndrome: an evaluation of patients who complain of dry mouth and dry eyes. Part 1: screening tests. Gerodontology 1996;13:35–43
23. Newman HN. Focal infection. J Dent Res 1996;75:1912–1919
24. Nagy-Newman K. Post operative restoration after surgery for oral malignancy. Chapter 17. In: Porter SR, Scully C, eds. Innovations and Developments in Non-Invasive Orofacial Health Care. Northwood: Science Reviews, 1996:225–229
25. Nagy K, Szöke I, Sonkodi I, et al. Inhibition of microflora associated with oral malignancy. Oral Oncol 2000;36:32–36
26. Peterson DE, Greenspan D, Squier CA. Oral infections in the immunocompromised host. Oral Pathol 1992;21:193–198
27. Eliasson L, Carlen A, Almstahl A, et al. Dental plaque pH and micro-organisms during hyposalivation. J Dent Res 2006;85: 334–338
28. Nagy KN, Sonkodi I, Szöke I, et al. The microflora associated with human oral carcinomas. Eur J Cancer 1998;34:304–308
29. Al-Nawas R, Grotz KA. Prospective study of the long term change of the oral flora after radiation therapy. Support Cancer Care 2006;14:291–296
30. McMillan AS, Tsang CS, Wong MC, et al. Efficacy of a novel lubricating system in the management of radiotherapy-related xerostomia. Oral Oncol 2006;42:842–848

Combined Surgical Excision and Radiation Therapy for Keloid Treatment

Sadanori Akita, MD, PhD,* Kozo Akino, MD, PhD,†
Aya Yakabe, MD,* Toshifumi Imaizumi, MD,*
Katsumi Tanaka, MD,* Kuniaki Anraku, MD,* Hiroki Yano, MD,*
Akiyoshi Hirano, MD*

Nagasaki, Japan

From the *Division of Plastic and Reconstructive Surgery and the †Division of Anatomy and Neurobiology, Department of Developmental and Reconstructive Medicine, Nagasaki University, Graduate School of Biomedical and Sciences, Nagasaki, Japan.

Address correspondence and reprint requests to Sadanori Akita, MD, PhD, Department of Plastic and Reconstructive Surgery, Nagasaki University, School of Medicine, 1-7-1 Sakamoto machi, Nagasaki, 8528501, Japan; E-mail: akitas@hf.rim.or.jp

This study was supported by grants from the Japanese Ministry of Education, Sports and Culture, #16390511, 16591795, 16659487, 16791091, 17659562, and 17659563.

Abstract: Various methods have been attempted for the treatment and management of keloids; however, there is little satisfactory clinical evidence in long-term follow ups. Also, there is a preference for occurrence and recurrence in anatomic location. Usually anatomic locations with higher regional tension and more sebaceous glands are inclined toward pathogenesis. Thirty-eight keloids treated with combined surgical excision and postoperative irradiation, using electron beams with only a 10-mm opening by lead shielding, were investigated at a mean follow up of 4.4 ± 2.5 years (range, 1–9 years) at a single institute. Ten locations such as the ear (n = 6), neck (n = 3), and upper lip (n = 1) were among the craniofacial locations. The hardness of the keloids and posttreatment scars was clinically and objectively tested with the Vancouver scar scale and a durometer, which is often used for the industrial measurement of thread balls and rubber. At a mean of 4.4 ± 2.5 years of follow up, the clinical characteristics of the scars were significantly better posttreatment as 2.6 ± 0.5 versus 1.0 ± 0.6, 3.7 ± 0.7 versus 1.7 ± 0.7, 2.9 ± 0.4 versus 1.3 ± 0.5, and 2.7 ± 0.5 versus 1.3 ± 0.5 (keloid scars versus posttreatment scars: pigmentation, pliability, height and vascularity, respectively, $P < 0.01$). The durometer readings were significantly lower posttreatment, 15.2 ± 3.9 versus 7.7 ± 2.9 (keloid scars versus posttreatment scars, $P < 0.01$). The recurrence rate was 21.2% overall with none in craniofacial locations. Therefore, the combined treatment of surgical excision and postoperative electron beam irradiation is effective for scar quality and reducing the recurrence rate in long-term follow up.

Key Words: Keloid, scar scale, durometer, combined surgical excision and radiation therapy, craniofacial location, long-term follow ups

The treatment of keloid scars combines several modalities, including surgery, corticosteroid or 5-fluorouracil injections, radiation, carbon dioxide laser, compression, silicone gel sheeting, and so on.[1–6] Treatment is performed individually or as a combination of several. Because the true mechanisms of keloid formation, progression, and pathogenesis have not been elucidated, clinical data have been collected and experimental investigations attempted.[7–9] The locations as well as racial and genetic, immunologic, and reactive causes of keloids seem to influence the therapeutic outcome, because stretched areas on the shoulders, elbows, suprapubic area, and midsternum all contain anatomic stretched forces. Craniofacial areas, especially in the ear, sometimes demonstrate the site of high frequency of keloids. Both keloids and hypertrophic scars demonstrate similar histologic, histochemical, and molecular patterns,[10] although their clinical manifestations and courses are relatively distinct.[5,11] Keloids are intractable to usual medical treatment and thus conservative modalities such as applying pressure devices or garments and chemical injections are adopted. In contrast, hypertrophic scars demonstrate profound characteristics during the course of maturation and progression. However, severe deformations occurring around functional body parts or visible keloid scars prevent patients from leading normal social lives as a result of psychologic distress as well as functional problems.[12] Here, efficient therapeutic modalities with combined surgical excision and postoperative electron beam irradiation were tested in a single institute in patients who were followed up for more than a 1-year postoperative observation period. The subjective and objective scores were evaluated for keloid signs and symptoms. Also, the hardness of the keloid scars was measured by the relative value of a durometer pre- and posttreatment, which is widely used for quality control of industrial threads or rubber.

Patients and Methods

Between April 1998 and March 2006, 32 patients (38 locations, 10 men and 22 women) who were treated with surgical excision and postoperative electron beam radiation with at least a 1-year follow-up period at Nagasaki University Hospital, Department of Plastic and Reconstructive Surgery, were included in this investigation. The average age was 38.9 ± 20.0 years (range, 11–76 years old) and the follow-up period was 4.4 ± 2.5 years (range, 1–9 years) after the final radiation. The locations of keloid scars were the anterior chest wall (n = 12), scapular and back (n = 8), abdomen and suprapubic (n = 6), ear (n = 6), neck (n = 3), upper limb (n = 2), and lip (n = 1). Previously treated and recurrent keloid scars consisted of four cases (two ears, two both anterior chest wall and abdomen) (Table 1). All scars were primarily excised surgically and electron beam radiation therapy followed. The surgical procedures included complete excision of the lesions followed by three-layer suture closure with subcutaneous undermining to minimize suture-site tension. Deeper layer of the fascia, the muscle or the periosteum, subcutaneous and dermal suturing was performed mainly by monofilament nylons or sometimes in the trunk and the extremities by PDS II (Ethicon; Johnson & Johnson K.K., Tokyo, Japan). Skin was closed with monofilament nylon or Steri-strip closure taping (3M Co., Ltd., Tokyo, Japan) unless skin was sutured. Radiation with a 9-MeV electron beam by a linear accelerator was administered in a 3.0 Gy/fraction with a 5-mm bolus booster to enhance energy concentration to the depth of skin at three fractions per week with at least a 1-day interval. Radiation was limited to a 10-mm wide

Table 1. Patient Profiles

Gender	Male:female = 10:22 (n = 32)
Age	38.9 ± 20.0 years (range, 11–76 years; median, 32 years)
Locations* (38 locations)	Anterior chest (n = 12)
	Scapular and back (n = 6)
	Abdomen and suprapubic (n = 6)
	Ear (n = 6)
	Neck (n = 3)
	Upper limb (n = 2)
	Lip (n = 1)

*Four patients (two ears and two both anterior chest and abdomen) had experienced previous treatment.

area by lead block protection of the sutures to eliminate adverse reactions in other body parts. The results were judged by the Vancouver scar scale in both subjective and objective manners by three evaluators who evaluated each other's patients in a blind fashion at least 1 year after wound healing. This was determined according to previously determined indices, which include pigmentation (0 = normal, 1 = hypopigmented, 2 = mixed, 3 = hyperpigmented), pliability (0 = normal, 1 = supple, 2 = yielding, 3 = firm, 4 = ropes, 5 = contracture), height (0 = flat, 1 = <2 mm, 2 = 2–5 mm, 3 = >5 mm), and vascularity (0 = normal, 1 = pink, 2 = red, 3 = purple).[13] Evaluation was confirmed by two other authors, who are scar specialists; therefore, each wound was assessed by three different evaluators. The results of each evaluator were blind and interevaluator difference was confirmed. The hardness pre- and posttreatment was also measured by a durometer, which is used for industrial products such as rubber thread rolls. The durometer used in this investigation was a TECLOCK GS-701N (TECLOCK, Co., Ltd., Nagano, Japan), which follows the international standard of SRIS 0101 and is defined as a spring instrument to measure hardness with a 5-mm diameter round noninvasive gauge head and a value range from 519 to 8379 mN (55–855 gf). The measurement of each point was always perpendicular to the scars and was repeated five times immediately after touching the scar and 30 seconds after touching, and the mean value of thee adjacent points at least 6 mm apart and 12 mm from the edge of intact skin was assessed at 25°C room temperature and 50% humidity with air conditioning following the manufacturer's instructions. Informed consent was obtained from all patients and there were no complications or complaints resulting from durometer measurements.

Table 2. Radiation Protocol

Start of radiation	4.0 ± 4.9 days (range, 1–24 days; median, 3 days)
Dose	19.2 ± 3.2 Gy (range, 15–30 Gy; median, 18 Gy)
Fraction	6.4 ± 1.3 times (range, 5–11 times; median, 6 times)
Duration	17.5 ± 8.5 days (range, 13–48 days; median, 14.5 days)
Follow up	4.4 ± 2.5 years (range, 1–9 years; median, 4 years)
Beam	9 MeV, 5-mm bolus, 10-mm wide shielding

STATISTICS

The results are expressed as mean ± standard deviation. The data between the two groups were evaluated by unpaired t test, and P values < 0.05 were considered statistically significant.

RESULTS

Timing and Dose of Electron Beam Radiation

After surgical excision, the scars of excised keloids were started on electron beam radiation therapy. The average day beginning was 4.0 ± 4.9 days (range, 1–24 days). All radiation therapy was fractionized at 3 Gy/fraction with at least 1 day of intermission. The total dose of radiation was 19.2 ± 3.0 Gy (range, 15–30 Gy) and the frequency of the fraction averaged 6.4 ± 1.3 times with a minimum five and maximum 11 fractions. Thus, the duration of electron beam radiation was 17.5 ± 8.5 days (minimum, 13 days; maximum, 48 days). Patients were hospitalized for at least 1 day after surgery. Some patients continued hospitalization until completion of radiation therapy; others visited the hospital as an outpatient. Some patients clinically demonstrated nausea and local heat after radiation; however, there was no cessation or cancellation of radiation therapy with 1 or 2 days of bedrest allowed after completion (Table 2). The earlier beginning of postradiation was observed in the last 5 years. The average age of 35.0 ± 16.3 years (median, 29 years) stared at 2.1 ± 1.1 days (range, 1–4 days; median, 2 days) after surgery in the last 5 years ($P < 0.05$ compared with the first 5-year group). Other parameters such as dose, fraction, and duration are identical to the total series (18.5 ± 1.2 Gy, 6.1 ± 0.3 times, and 14.3 ± 1.4 days dose, fraction, and

Table 3. Radiation Protocol in the Last 5 Years (n = 19)

Gender	Male:female = 6:13 (n = 19)
Age	35.0 ± 16.3 years (range,11–63 years; median, 29 years)
Start of radiation	2.1 ± 1.1 days (range, 1–4 days; median, 2 days)
Dose	18.5 ± 1.2 Gy (range,18–21 Gy; median, 18 Gy)
Fraction	6.1 ± 0.3 times (range, 6–7 times; median, 6 times)
Duration	14.3 ± 1.4 days (range, 13–17 days; median, 14 days)
Follow up	2.6 ± 1.4 years (range, 1–5 years; median, 2 years)

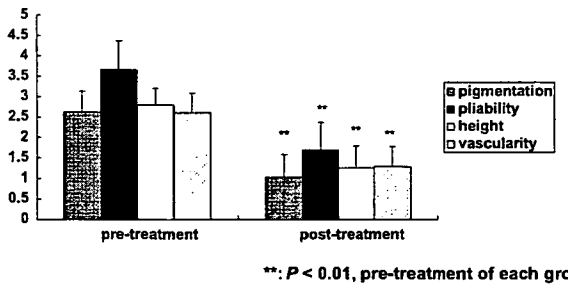

Fig 1 Vancouver scar scale: measurements were repeated by three different evaluators in a blind fashion and the average value was taken. Pigmentation: pretreatment scars were 1.0 ± 0.6, whereas posttreated scars were 2.6 ± 0.5 ($P < 0.01$). Pliability: pretreatment scars were 1.7 ± 0.7, whereas posttreated scars were 3.7 ± 0.7 ($P < 0.01$). Height: pretreatment scars were 1.3 ± 0.5, whereas posttreated scars were 2.8 ± 0.4 ($P < 0.01$). Vascularity: pretreatment scars were 1.3 ± 0.5, whereas posttreated scars were 2.7 ± 0.5 ($P < 0.01$).

duration, respectively), although there was significantly shorter follow up (2.6 ± 1.4 years; range, 1–5 years; median, 2 years) in the last 5 years ($P < 0.01$ compared with the first 5-year group; $P < 0.02$ compared with the total patient group) (Table 3).

Scar Scale

The scar scale demonstrated significantly better improvement in all categories of pigmentation, pliability, height, and vascularity after treatment. The pigmentation was 2.6 ± 0.5 pretreatment and 1.0 ± 0.6 posttreatment ($P < 0.01$). The pliability improved 3.7 ± 0.7 to 1.7 ± 0.7 from pretreatment to posttreatment ($P < 0.01$). The height of the scar changed from 2.8 ± 0.4 to 1.3 ± 0.5 and the vascularity from 2.7 ± 0.5 to 1.3 ± 0.5 (Fig 1). There was no significant difference among three evaluators on behalf of each parameter analysis.

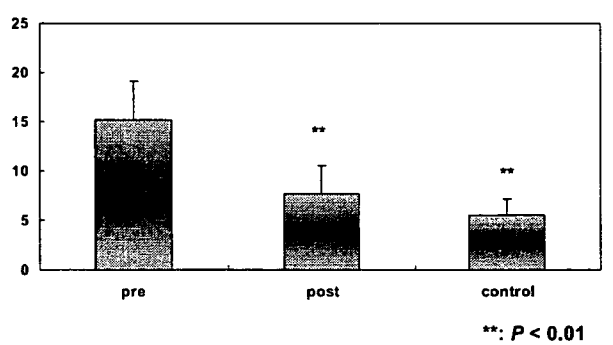

Fig 2 Durometer reading. The average durometer reading was 15.2 ± 3.9, 7.7 ± 2.9, and 5.5 ± 1.6 pretreatment, posttreatment, and control, which is a nonscar reading in comparable anatomic locations of the measurement ($P < 0.01$).

Table 4. Recurrence Rate

Anterior chest (n = 12)	3/12	25.0%
Scapular and back (n = 8)	3/8	37.5%
Abdomen and suprapubic (n = 6)	2/6	33.3%
Ear (n = 6)	0/6	0%
Neck (n = 3)	0/3	0%
Upper limb (n = 2)	0/2	0%
Lip (n = 1)	0/1	0%
	8/38	21.1%

Durometer Reading

The average durometer reading was 15.2 ± 3.9, 7.7 ± 2.9 and 5.5 ± 1.6, pretreatment, posttreatment, and control ($P < 0.01$) (Fig 2), of which scar hardness was consistent to the previous measurement in burn scars.[14]

Recurrence Rate

In the anterior chest wall locations, three of 12 keloids demonstrated clinical recurrence, of which one was a recurrent case. Three of eight cases of the scapular and back also demonstrated clinical recurrence of keloids, whereas there was recurrence in two of six cases of the lower abdomen and suprapubic. One patient, who demonstrated keloids in both the anterior chest and abdomen, and was previously treated with radiation, developed a keloid. There was no recurrence in ear locations. The total recurrence rate after surgical excision and radiation therapy was 21.1% (eight in 38 keloids) (Table 4). In the last 5 years, there was a significantly reduced recurrence rate. Only two of 23 locations were of keloid and total recurrence rate of this population is 8.7%. Although a longer period of the follow up should be traced in last 5-year group, the majority of the recurrence occurred within 2 years after treatment in the total series. Only

Table 5. Recurrence Rate in the Last 5 Years

Anterior chest (n = 6)	1/6	16.7%
Scapular and back (n = 4)	0/4	0%
Abdomen and suprapubic (n = 2)	1/2	50%
Ear (n = 6)	0/6	0%
Neck (n = 2)	0/2	0%
Upper limb (n = 2)	0/2	0%
Lip (n = 1)	0/1	0%
	2/23	8.7%

one patient with a neck keloid was followed up over 5 years in the craniofacial region and the other nine patients were followed up on average 2.7 ± 1.6 years (mean, 3.5 years) (Table 5).

Discussion

Keloids are intractable to various therapeutic interventions. The usefulness of electron beams has been reported, and combined surgical excision improves the overall excellent outcome, complete response, and reduction recurrence rate[8,15,16] in nonwhite populations. Although the detailed mechanism of radiation is still unclear, alteration of fibroblasts in keloid alpha-1/beta-1 integrin collagen receptor expression and the pathway is proposed,[17] electron beams are effective in the interleukin-6 signaling pathway of keloid fibroblasts, which was confirmed by global gene expression analysis.[18]

In our series, clinical parameters depicted by the Vancouver scar scale demonstrated significant therapeutic effects posttreatment. Pigmentation is sometimes a concern after radiation therapy[19]; however, no such complications increased after treatment. There is a possibility of carcinogenesis in anecdotal case reports,[20] but there was no tumor progression in our series.

Objective evaluation using a durometer demonstrated significantly softer scars after treatment. This method may become more widely applicable to measure scar quality.[14]

The recurrence rate after combined surgical excision and postoperative electron beam radiation varied from 8% to 71%.[8,15,16,19] Our data demonstrated 21.1%, which is comparable to the same racial background populations.[8] In detailed analysis of our treatment series by dividing the first and last 5-year periods, the most significantly changed parameter was the beginning of the postsurgical radiation. In the last 5 years, first radiation was performed at an average of 2.1 days after surgery. Considering the other parameters are almost identical to total series, the earlier beginning of radiation should be taken as a standardized protocol.

The suture materials are also a concern. The nonabsorbable materials are used for subcutaneous and dermal suturing, especially in the craniofacial region. The most important factor may be how to reduce the tension around the suture margins and how to avoid violating the shallower layer of the dermis because the hyaluronan content is less when the papillary layer of the dermis is damaged[21] and histopathologically remarked changes are observed in the upper layer of the reticular dermis.[22] Thus, dermal suturing of nonabsorbable materials should be applied to the deeper reticular dermis.

Ear keloids are considered differently from other keloids, because the required dose of radiation seems lower and cellular responsiveness is more prone to normal fibroblasts[23]; further determination of radiation doses and vehicle should be investigated. However, other craniofacial locations such as the neck and upper lip also demonstrated no recurrence rate as did the ear, and it should be noted that combined surgical excision and postoperative electron beam irradiation are especially effective in these locations.

In long-term observation averaging more than 4 years posttreatment, combined surgical excision and electron beam radiation, which was started within a few days, are very beneficial in controlling scar quality and preventing recurrence.

References

1. Al-Attar A, Mess S, Thomassen JM, et al. Keloid pathogenesis and treatment. Plast Reconstr Surg 2005;117:286–300
2. Muneuchi G, Suzuki S, Onodera M, et al. Long-term outcome of intralesional injection of triamcinolone acetonide for the treatment of keloid scars in Asian patients. Scand J Plast Reconstr Surg Hand Surg 2006;40:111–116
3. Uppal RS, Khan U, Kakar S, et al. The effects of a single dose of 5-fluorouracil on keloid scars: a clinical trial of timed wound irrigation after extralesional excision. Plast Reconstr Surg 2001;108:1218–1224
4. Norris JE. The effect of carbon dioxide laser surgery on the recurrence of keloids. Plast Reconstr Surg 1991;87:44–49
5. Darzi MA, Chowdri NA, Kaul SK, et al. Evaluation of various methods of treating keloids and hypertrophic scars: 10-year follow-up study. Br J Plast Surg 1992;45:374–379
6. Linares HA, Larson DL, Willis-Galstaun BA. Historical notes on the use of pressure in the treatment of hypertrophic scars or keloids. Burns 1993;19:17–21
7. Ragoowansi R, Cornes PG, Moss AL, et al. Treatment of keloids by surgical excision and immediate postoperative single-fraction radiotherapy. Plast Reconstr Surg 2003;111: 1853–1859
8. Ogawa R, Mitsuhashi K, Hyakusoku H, et al. Postoperative electron-beam irradiation therapy for keloids and hypertrophic scars: retrospective study of 147 cases followed for more than 18 months. Plast Reconstr Surg 2003;111:547–553
9. Garg MK, Weiss P, Sharma AK, et al. Adjuvant high dose rate brachytherapy (Ir-192) in the management of keloids which have recurred after surgical excision and external radiation. Radiother Oncol 2004;73:233–236
10. Alster TS, Tanzi EL. Hypertrophic scars and keloids: etiology and management. Am J Clin Dermatol 2003;4:235–243
11. Rahban SR, Garner WL. Fibroproliferative scars. Clin Plast Surg 2003;30:77–89
12. Copcu E, Sivrioglu N, Oztan Y. Combination of surgery and intralesional verapamil injection in the treatment of the keloid. J Burn Care Rehabil 2004;25:1–7
13. Baryza MJ, Baryza GA. The Vancouver scar scale: an adminis tration tool and its interrater reliability. J Burn Care Rehabil 1995;16:535–538
14. Akita S, Akino K, Imaizumi T, et al. A basic fibroblast growth

factor improved the quality of skin grafting in burn patients. Burns 2005;31:855–858
15. Kovalic JJ, Perez CA. Radiation therapy following keloidectomy; a 20-year experience. Int J Radiat Oncol Biol Phys 1989;17:77–80
16. Ollstein RN, Siegel HW, Gillooley JF, et al. Treatment of keloids by combined surgical excision and immediate postoperative x-ray therapy. Ann Plast Surg 1981;7: 281–285
17. Szulqit G, Rudolph R, Wandel A, et al. Alterations in fibroblast alpha1 beta1 integrin collagen receptor expression in keloids and hypertrophic scars. J Invest Dermatol 2002;118:409–415
18. Tosa M, Ghazizadeh M, Shimizu H, et al. Global gene expression analysis of keloid fibroblasts in response to electron beam irradiation reveals the involvement of interleukin-6 pathway. J Invest Dermatol 2005;124:704–713
19. Borok TL, Bray M, Sinclair I, et al. Role of ionizing irradiation for 393 keloids. Int J Radiat Oncol Biol Phys 1988;15: 865–870
20. Botwood N, Lewanski C, Lowdell C. The risk of treating keloids with radiotherapy. Br J Radiol 1999;72:1222–1224
21. Bertheim U, Hellstrom S. The distribution of hyaluronan in human skin and mature, hypertrophic and keloid scars. Br J Plast Surg 1994;47:483–489
22. Lee JY, Yang CC, Chao SC, et al. Histopathological differential diagnosis of keloid and hypertrophic scar. Am J Dermatopathol 2004;26:379–384
23. Lim IJ, Phan TT, Song C, et al. Investigation of the influence of keloid-derived keratinocytes on fibroblast growth and proliferation in vitro. Plast Reconstr Surg 2001;107:797–808

Peripheral Osteoma of the Maxillary Alveolar Process

Ioannis A. Iatrou, MD, DDS, DrDent,
Minas D. Leventis, DDS, MSc, Panayotis E. Dais, DDS,
Konstantinos I. Tosios, DDS, DrDent

Athens, Greece

Abstract: Osteoma is a benign, slow-growing tumor characterized by proliferation of compact or cancellous bone. Solitary osteomas are classified as peripheral, central, or extraskeletal. Peripheral osteomas of the oral cavity are unusual and the maxilla is rarely affected. They manifest as asymptomatic, fixed tumors of bony-hard consistency that may be sessile or pedunculated. Radiographically, a well-circumscribed round or oval radiopaque mass is seen that is microscopically composed of cancellous or trabecular bone. A case of a compact, peripheral osteoma arising from the buccal plate of the alveolar ridge of the maxilla in a 64-year-old patient is presented. According to our literature review, this is the seventh case reported in the maxillary ridge.

From the Department of Oral Pathology and Surgery, Faculty of Dentistry, University of Athens, Athens, Greece.

Address correspondence and reprint requests to Ioannis A. Iatrou, MD, DDS, Associate Professor of Oral and Maxillofacial Surgery, Department of Oral Pathology and Surgery, Faculty of Dentistry, University of Athens, 2 Thivon Street, 11527, Athens, Greece; E-mail: iiatrou@dent.uoa.gr

Key Words: Osteoma, peripheral, bone tumors, maxilla, maxillary tumors

Osteoma is a benign, slow-growing tumor characterized by proliferation of compact or cancellous bone.[1,2] Solitary osteomas are classified as peripheral, central, or extraskeletal.[3] Peripheral and central osteomas arise from the periosteum or the endosteum, respectively. Extraskeletal osteomas develop within soft tissue, usually striated muscles, and are considered choristomas. Osteomas may be solitary or multiple, the latter mainly associated with Gardner's syndrome.[2–5]

Peripheral osteomas are found almost exclusively in the skull and maxillofacial bones. The most common site is the frontal sinus followed by the ethmoidal and maxillary sinuses. Osteomas of the oral cavity are unusual and the maxilla is rarely affected.[5–7] There is no age or sex predilection.[2,5] Clinically, they manifest as fixed tumors of bony-hard consistency that may be sessile or pedunculated. Because osteomas are usually asymptomatic, most patients present because of aesthetic considerations such as facial asymmetry or malocclusion. Pain, gagging, nausea, and dysphagia are rarely reported.[4,5]

Radiographically, the lesion appears as a well-circumscribed round or oval radiopaque mass.[3,8,9] Histologically, an osteoma may be composed of dense cortical bone (compact or ivory osteoma) or trabecular, medullary bone (cancellous, trabecular, or spongy osteoma).[5] When fibrous connective tissue dominates the microscopic picture, the lesion is called fibroosteoma or fibrous osteoma.[10]

A rare case of compact, peripheral osteoma arising from the buccal plate of the alveolar ridge of the maxilla in a 64-year-old patient is presented.

Clinical Report

A 64-year-old white woman was referred by her periodontologist for evaluation of a painless swelling on the buccal plate of the right maxillary alveolar ridge. According to the patient, the lesion had been present for several months, and there was no history of trauma or inflammation to the area. Her medical history was noncontributory.

Oral examination revealed a circumscribed tumor on the alveolar maxillary ridge, buccally to the missing second premolar tooth (Fig 1). The

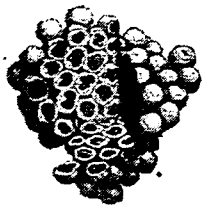

STEM CELLS®

Acceleration of Sensory Neural Regeneration and Wound Healing with Human Mesenchymal Stem Cells in Immunodeficient Rats

Toshifumi Imaizumi, Sadanori Akita, Kozo Akino and Akiyoshi Hirano

Stem Cells 2007;25;2956-2963; originally published online Aug 16, 2007;
DOI: 10.1634/stemcells.2007-0187

STEM CELLS®, an international peer-reviewed journal, covers all aspects of stem cell research: embryonic stem cells; tissue-specific stem cells; cancer stem cells; the stem cell niche; stem cell genetics and genomics; translational and clinical research; technology development.

STEM CELLS® is a monthly publication, it has been published continuously since 1983. The Journal is owned, published, and trademarked by AlphaMed Press, 318 Blackwell Street, Suite 260, Durham, North Carolina, 27701. © 2007 by AlphaMed Press, all rights reserved. Print ISSN: 1066-5099. Online ISSN: 1549-4918.

AlphaMed Press

STEM CELLS®

TRANSLATIONAL AND CLINICAL RESEARCH

Acceleration of Sensory Neural Regeneration and Wound Healing with Human Mesenchymal Stem Cells in Immunodeficient Rats

TOSHIFUMI IMAIZUMI,[a] SADANORI AKITA,[a] KOZO AKINO,[b] AKIYOSHI HIRANO[a]

Divisions of [a]Plastic and Reconstructive Surgery and [b]Anatomy and Neurobiology, Department of Developmental and Reconstructive Medicine, Nagasaki University, Graduate School of Biomedical and Sciences, Nagasaki, Japan

Key Words. Human mesenchymal stem cell • Nude rat • Green fluorescent protein • Tracking • Differentiation Fibroblast growth factor • Vascularized epigastric flap • Lower extremity wound healing

ABSTRACT

The sensory nerve is highly involved in lower extremity wound healing. In diabetic and vascular diseases, impaired nerve function and blood flow delay wound healing. Tissue regeneration using adult stem cells is a targeted therapeutic modality in disorders of nerve and blood supply. Effective delivery using an autologous vascularized fascial flap as a vehicle of stem cells leads to severed sensory nerve recovery, local tissue blood flow, and wound healing. Human MSCs (hMSCs) were transfected with green fluorescent protein (GFP) cDNA and tested for efficiency and proliferation in vitro. The nude rat model with femoral vessel and saphenous nerve severance and ligation was wrapped with a vascularized epigastric flap for GFP-hMSC, fibroblast growth factor-2 (FGF-2), or a combination of both after 2 weeks. Maximum nerve conduction velocity recovered to 70% of the presurgical level in the GFP-hMSC- and FGF-2-treated group at 2 weeks. Blood flow and nerve conduction velocity were positively correlated at 1 week. Wound healing in the ipsilateral paw had significantly improved by 1 week. Histologically, blood vessels and nerves are very organized, and regenerated neuron immunoreactivity of GAP-43 and a nerve regrowth marker of S-100 were remarkable in the human GFP (hGFP)-hMSC and FGF-2-treated group at 2 weeks; therefore, sensory nerve regeneration, blood flow, and wound healing were improved by the administration of stem cells and FGF-2 via a vascularized flap. This may be implicated in clinical denervated and reduced circulation tissue wound healing. STEM CELLS *2007;25:2956–2963*

Disclosure of potential conflicts of interest is found at the end of this article.

INTRODUCTION

Denervation or the impairment of motor, sympathetic, or sensory nerves may result in delayed skin wound healing [1–3]. Nerve repair or regeneration has been attempted by various methods, including immediate end-on-end repair with brain-derived neurotrophic factor [4] and thin-walled nerve guide or autologous nerve graft [5]. Among these peripheral nerve regenerations, stem cell transplantation may be a future modality. Skin-derived stem cells are able to regenerate nerves with nerve guides [6], whereas bone marrow mesenchymal stem cells in vitro are able to express glial markers and induce nerve regeneration with glial growth factor [7]. Peripheral nerve involvement in healing problems was demonstrated in an experimental model of the rabbit medial collateral ligament [8]. Also, peripheral nerve impairment directs neuropathy and is worsened with ischemic physical conditions. Reduced sensation, as well as motor or autonomic deficits, may lead to diabetic neuropathy and ulcers [9].

In lower peripheral nerve impairment, clinical saphenous nerve injuries are sometimes accompanied with a saphenous vein stripping procedure and objectively assessed with clinical symptoms [10], causing sensory disturbances in the medical thigh, knee, calf, and sole, as well as instability of these inner lower extremity structures due to loss of motor nerve government. In this regard, investigation of the involvement of the saphenous nerve in sole wound healing may bring about insight into the role of the peripheral nerve in in vivo wound healing with clinical relevance.

Fibroblast growth factors (FGFs), especially FGF-2 or basic FGF, hasten nerve regeneration after sciatic nerve crush by proliferating Schwann cells, inducing axonal growth, and prohibiting remyelination in a transgenic mouse model [11]. Schwann cells overexpressing the FGF-2 isoform successfully improve peripheral nerve regeneration when cells are grafted with Matrigel (BD Biosciences, San Diego, http://www.bdbiosciences.com) [12].

Human mesenchymal stem cells proliferate in culture with attached well-spread fibroblast-like cell morphology [13]. The growth kinetics and differentiation were studied with human mesenchymal stem cells in subcultivation, followed by cryopreservation [14]. The early phase of cell profiles and the expression pattern by cytokines of the human mesenchymal stem cells were investigated in vitro [15]. Bone marrow derived human MSCs (hMSCs) are stringently sorted by cell surface antigen markers to exclude hematopoietic markers such as CD14, CD45, and CD34 and include mesenchymal markers such as CD105, CD166, CD29, and CD44 [13, 14]. Mesenchymal stem cells have the capacity to differentiate and regenerate nerves under certain conditions [16] and are available for supporting nerve regeneration and myelination in rats when transdifferentiated mesenchymal stem cells are grafted [17].

Correspondence: Sadanori Akita, M.D., Ph.D., Nagasaki University, School of Medicine, 1-7-1 Sakamoto Machi, Nagasaki 8528501, Japan. Telephone: +81-95-849-7327; Fax: +81-95-849-7330; e-mail: akitas@hf.rim.or.jp Received March 20, 2007; accepted for publication July 9, 2007; first published online in STEM CELLS *EXPRESS* August 16, 2007. 1066-5099/2007/$30.00/0 doi: 10.1634/stemcells.2007-0187

The hMSCs are able to differentiate into bone in cranial bone defects and ectopic bone formation with an appropriate cell carrier and cytokines [18, 19]. The superficial epigastric fascial flap used in the ectopic bone formation model is an ideal tool for transferring hMSCs and cytokines. As hMSCs and FGF-2 separately induce peripheral nerve regeneration, combined treatment may be more efficient for nerve regeneration. The saphenous nerve severing and ligating model was tested for nerve regeneration by hMSC and FGF-2 administration via a vascularized epigastric flap, and sole wound healing was also investigated.

MATERIALS AND METHODS

Human Mesenchymal Stem Cells

Human mesenchymal stem cells from a single human bone-marrow donor were isolated by density gradient centrifugation and were strictly sorted as positive for markers such as CD105, CD166, CD29, and CD44 and negative for cell surface markers such as CD14, CD34, and CD45. These hMSCs were purchased from Lonza Walkerville, Inc. (Walkersville, MD, http://www.lonzabioscience.com), and cryopreserved cells were thawed immediately according to the manufacturer's instructions. Two independent donor-derived hMSCs (white female; lots 1F0658 and 1F1061) were used in the experiments. The cells were cultured in "basic medium" of Dulbecco's modified Eagle's medium (DMEM) containing low glucose supplemented with 10% fetal bovine serum (FBS) (heat-inactivated; Gibco, Tokyo, http://www.invitrogen.com), 200 mM L-glutamine, and penicillin (100 U/ml) and streptomycin (100 μg/ml) at 37°C in 95% humidified air and 5% CO_2. The medium was changed every 3 days until the cells reached approximately 80%–90% of total confluence, and then the cells were passaged up to three times. Growth characteristics during the four passages in FBS were indistinguishable. The cells were washed using 10 ml of phosphate-buffered saline (PBS) and then liberated by exposure to 0.25% trypsin/1 mM EDTA (Gibco) for 3 minutes at 37°C, followed by tapping the dishes and the addition of 5 ml of culture medium. The cells were centrifuged at 400*g* and then resuspended in basic medium for the following in vitro examinations. The other cells were stored at −70°C until used in a solution containing 5% human serum albumin (IS Japan, Co., Ltd., Saitama, Japan, http://www.isjpn.co.jp) and 10% dimethyl sulfoxide (Sigma-Aldrich, Tokyo, http://www.sigmaaldrich.com) according to the manufacturers' instructions. Cells were counted three times using a Beckman Coulter Cell and Particle Counter (Beckman Coulter, Tokyo, http://www.beckmancoulter.com).

GFP-hMSC Cell Preparation

hMSCs (5×10^4) were seeded into 24-well plates with 500 μl of DMEM containing low glucose supplemented with 10% FBS, without antibiotics, at approximately 90% confluence overnight. The next day, 1 μl of gently mixed Lipofectamine 2000 (Invitrogen, Carlsbad, CA, http://www.invitrogen.com) was diluted in 50 μl of Opti-MEM-1 Reduced Serum Medium (Invitrogen). One μg of green fluorescent protein (GFP) DNA plasmid (pIRES-EGFP) (Clontech, Mountain View, CA, http://www.clontech.com), which contains human cytomegalovirus promoter, enhanced green fluorescent protein gene, and the bovine growth hormone poly(A) signal, was mixed with 50 μl of Opti-MEM-1 Reduced Serum Medium. Immediately, another 50 μl of Opti-MEM-1 Reduced Serum Medium was added to each well containing 50 μl of Opti-MEM-1 Reduced Serum Medium with Lipofectamine 2000. After a 5-minute incubation, the complex of plasmid and Lipofectamine 2000 was left at room temperature for 20 minutes and then added to each well of cells with gentle rocking. The complex-added wells were incubated for 3, 6, 18, or 24 hours at 37°C. The medium was changed to basic medium supplemented with 50 mg/ml Geneticin (G-418 sulfate; Gibco) instead of penicillin (100 U/ml) and streptomycin (100 μg/ml) for cell selection. The cell culture continued for 4 days before the first passage (P1), and G-418-added medium was continued for 3 weeks for complete selection of cells. The passage was repeated when cells reached 80%–90% confluence in each culture plate. Transfection efficacy was confirmed by fluorescent microscopy, and fluorescent cells were counted five times under each condition. DNA experiments followed the Nagasaki University Safety Committee guidelines for handling recombinant DNA, which were approved on July 4, 2002 (no. 0207040655).

GFP-Transfected hMSC Cell Growth Curve in Passage

After cells were successfully transfected with GFP DNA plasmid, the growth curve was tested from day 0 at the time of cell culture to day 3 to determine the best efficiency of cell transfection and proliferation.

FGF-2

Genetically recombinant human FGF-2 (Trafermin) was purchased from Kaken Pharmaceutical Co. Ltd (Tokyo, http://www.kaken.co.jp/english). Freeze-dried samples were dissolved in PBS and dissolved in culture medium 30 minutes before in vitro use. The concentration of basic FGF (bFGF) was within the physiological range, according to the manufacturer's instructions.

Animal Protocol

Fifty male F344/NJCl-rnu nude rats, ages 8–9 weeks and weighing 250–300 g, that were deficient in T-cell function, were used in this experiment. Animals were obtained from CLEA Japan (Tokyo, http://www.clea-japan.com) and housed in the laboratory animal center for biomedical research (Nagasaki University School of Medicine, Nagasaki, Japan), and the protocol of the animal experiment was approved by the Institutional Animal Care and Use Committee of Nagasaki University (0308150310). They were handled according to the guidelines established for animal care at the center. Each rat had free access to both sterile water and standard rodent soft chow ad libitum.

Surgical Procedure

Rats were anesthetized with 40 mg/kg body weight intraperitoneal injection of pentobarbital sodium, United States Pharmacopeial Convention (Nembutal) (Abbott, Abbott Park, IL, http://www.abbott.com). The animals were then placed in the supine position, and initially, a 4 × 4 cm^2 axial-pattern fasciocutaneous flap was made. All of the branches from the flap pedicle (superficial epigastric artery and veins) were kept intact. After flap elevation, the cutaneous portion was removed, and the remaining pedicled fascial flap was then used to wrap the transected saphenous nerves and femoral vessels and for subsequent cell and cytokine delivery [20]. The actual size of the flap used for wrapping was 1.5 × 1.5 cm^2, and both vessels and nerves were totally wrapped with the fascial (connective tissue) portion. All animals received 0.1 ml of DMEM containing either 5×10^6 GFP-transfected hMSCs, bFGF (10 μg), combined administration of the two, or vehicle of DMEM alone within 30 minutes prior to injection. Injection of the above solutions was into the proximal site of the femoral artery and veins, where the superficial epigastric vessels originate, after the distal site of the bifurcated femoral artery to the epigastric artery and veins was clamped, where the severed femoral artery and veins were also wrapped with a vascularized flap. All clamps were removed after a 10-minute incubation of the injection, as described previously [20]. Severance and ligation of the femoral vessels and saphenous nerve were confirmed by using 3-0 nylon on both proximal and distal stumps.

Rats were divided into the following groups:

1. No-reconstruction group ($n = 10$): no reconstruction after severing and ligating both saphenous nerve and femoral vessels.
2. Control group (vascularized epigastric flap alone) ($n = 10$): 5 μl of DMEM was added through the superficial epigastic artery.
3. hMSC treatment group ($n = 10$): 5 μl of DMEM solution containing 5×10^6 GFP-transfected hMSCs was prepared 30 minutes before transplantation for each epigastric flap.
4. FGF-2 group ($n = 10$): 5 μl of DMEM solution containing 10 μg of FGF-2 was prepared 30 minutes before transplantation for each epigastric flap.

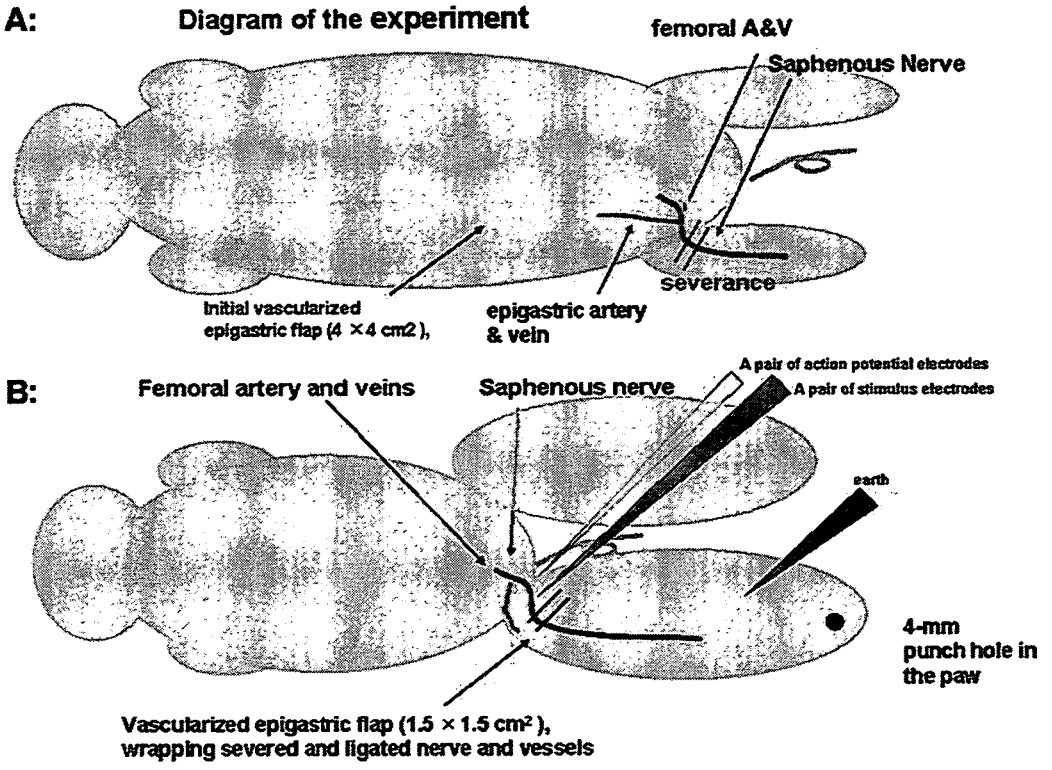

Figure 1. Diagram of the experiment. **(A):** Vascularized fasciocutaneous flap and severance of the nerve and artery. A 4 × 4 cm^2 fasciocutaneous flap, which is a vascularized superficial epigastric flap bifurcated from the proximal femoral artery, was elevated, and the femoral artery peripheral to the superficial epigastric artery and saphenous nerve was severed and ligated. **(B):** Wrapping the severed nerve and artery with vascularized epigastric flap and creation of 4-mm diameter punch hole in the paw. After removal of the circumferential excessive tissue and skin portion of the flap, the severed nerve and artery were wrapped with a reduced-size 1.5 × 1.5 cm^2 vascularized flap. Nerve conduction velocity was measured just proximal to the severance, with a pair of stimulus electrodes distally and a pair of action potential electrodes proximally. A 4-mm diameter punch hole was created in the ipsilateral foot. Abbreviation: A&V, artery and veins.

5. Combined group (n = 10): both 5 × 10^6 GFP-transfected hMSCs and 10 μg of FGF-2 were prepared 30 minutes before transplantation for each epigastric flap.

Blood flow was measured using a noncontact laser blood flowmeter (ALF 21N; Advance Co. Ltd, Tokyo, http://www.advance.jp/english). The maximum sensory nerve conduction velocity was determined with a digital stimulator (model PG4000A; Cygnus Technology, Inc., Delaware Water Gap, PA, http://www.cygnustech.com) and a gated constant current source stimulus isolator (model SIU90; Cygnus Technology) and amplified with a differential extracellular amplifier (model ER-1; Cygnus Technology). Needle electrodes were set with a 5-mm gap at the saphenous nerve after meticulous dissection from other tissues under a microscope, and all nerve experiments were shielded by a magnetic shield cage (Astec Co., Ltd., Fukuoka, Japan, http://www.astec.com). The "earth" of the needles was inserted into the distant lower calf, and a pair of excitation needles and a pair of collection needles were placed with a 5-mm gap for velocity measurement. All blood flow data and nerve conduction velocity data were immediately transferred to an Analogue-Digital converter of PowerLab/4ST (ML 750; ADInstruments Japan Inc., Nagoya, Japan, http://www.adinstruments.com), and data were analyzed with the accompanying software of Scope v3.7 for nerve conduction and Chart v4.2.3 for blood flow.

Data samplings were repeated five times, and the mean value for each animal was adopted for further group analyses. Measurements were performed at the distal periphery of the severed nerves and vessels preligation (10 animals per group), immediately after ligation (10 animals per group), at 1 week (5 animals per group), and at 2 weeks (5 animals per group).

After terminating blood flow and maximum nerve conduction velocity experiments, inguinal wounds were sutured with 5-0 nylon, and an ipsilateral foot paw wound was created with 4-mm punch biopsy instruments. The wounds were covered with transparent semipermeable membranes (Cathereep Flexible, Soft & Smooth roll, number 1510; Nichiban Co., Ltd., Tokyo. http://www.nichiban.co.jp/medical). The experimental diagram of nerve severance, vessel ligation, vascularized flap wrapping, blood flow, and nerve velocity measurement is shown in Figure 1.

Wound sizes were photographed in the supine position using a 600 million dots-per-inch digital camera (Cyber-shot; Sony, Tokyo, http://www.sony.com) and an image analyzer (NIH Image, version 1.62) on a Macintosh computer. The macroscopic size of the remaining wound was calculated three times for each group of five animals at 1, 3, 7, and 14 days following the previous wound healing experiment [21].

Animals were kept at a constant room temperature of 25°C with 55% humidity, and ankle body temperature was measured using a noncontact thermometer (UNIVLOT, UT-2) at the beginning and end of experiments. Animals were euthanized at 1 (five animals per each group) and 2 (five animals per each group) weeks postoperatively. Sections including the possible reconstructed nerve and vessels were fixed in 4% paraformaldehyde solution and processed for H&E for histology and immunohistochemistry.

Histology

Specimens were fixed in cold 4% paraformaldehyde solution for 2 weeks, decalcified in EDTA, embedded in paraffin, and cut into 5-μm-thick sections. Slides were stained with H&E.

Immunohistochemistry

For axonal regeneration marker analysis, immunostaining for growth-associated protein (GAP)-43, the mouse monoclonal GAP-43 antibody (catalog no. sc-33705; Santa Cruz Biotechnology Inc., Santa Cruz, CA, http://www.scbt.com) was used. This GAP-43 antibody was raised against full-length GAP-43 of rat origin and

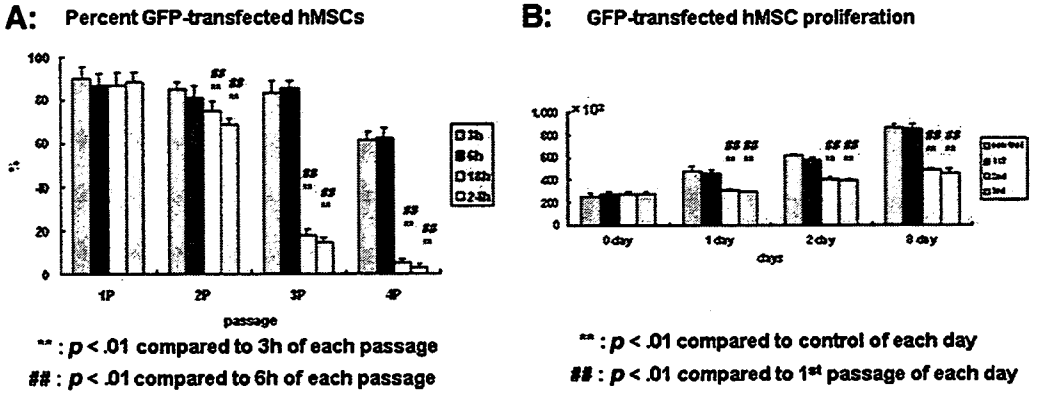

Figure 2. Efficiency of the GFP gene in hMSCs and proliferation. (**A**): hMSCs were transfected with the GFP gene at various incubation times. The highest transfection efficiency was with either 3- or 6-h incubation and up to three Ps. (**B**): The cell proliferation curve after GFP transfection was followed up to day 3. There was a significance between P1 cells and P2 or P3 cells from day 1 to day 3 ($p < .01$). There was no significant cell proliferation between control (no human GFP transfection) and P1 cells at any time point. Abbreviations: GFP, green fluorescent protein; h, hour; hMSC, human MSC; P, passage.

was able to detect axonal membranous protein of rats, mice, and humans. The primary antibody was incubated overnight at a dilution of 1:50 by PBS per the manufacturer's recommendations, at 4°C, followed by a rabbit anti-mouse IgG rhodamine-conjugated secondary antibody (catalog no. AP160R; Chemicon, Temecula, CA, http://www.chemicon.com) at 1:500 for 1 hour at room temperature and 4',6-diamidinophenylindole dihydrochloride (DAPI) for nuclear DNA counterstaining DAPI (catalog no. 340-07971; Dojindo Molecular Technologies Inc., Kumamoto, Japan, http://www.dojindo.com) at 1:100 for 1 hour at room temperature.

For detection of the regenerated nerve fiber, S-100 immunohistochemistry was performed. Rabbit polyclonal anti-S-100 antibody (catalog no. N1573, ready-to-use; Dako Japan Inc., Kyoto, Japan, http://www.dako.com) was incubated overnight at room temperature, and then the anti-rabbit Histofine simple stain MAX PO kit (code 414151F; Nichirei, Tokyo, http://www.nichirei.co.jp/english/index.html) followed as a universal immunoenzyme polymer method according to the manufacturer's instructions with diaminobenzamine chromogen, and finally hematoxylin staining was used for counterstaining. All fluorescent analyses were performed using the Lumina Vision (Mitani Corporation, Fukui, Japan, http://www.mitani-corp.co.jp) bioimaging analysis system for GFP (green), DAPI (blue), and GAP-43 (red).

Statistical Analysis

The results of the percentage of hGFP-positive hMSCs and GFP-hMSC proliferation analyses are expressed as the means ± SD. Data were statistically compared with unpaired *t* test, and *p* values less than 0.05 were considered significant.

RESULTS

DNA Transfection Efficiency

The percentage of transfection efficiency of GFP to hMSCs was investigated with 3-, 6-, 18-, and 24-hour incubations before cell selection and each passage from P1 to P4. The 3- and 6-hour incubations demonstrated statistical significance from P2 to P3 compared with 18- and 24-hour incubations (90.3% ± 5.3%, 87.1% ± 5.0%, 86.8% ± 5.8%, 88.1% ± 4.6%, 85.1% ± 3.4%, 81.5% ± 5.4%, 74.9% ± 4.8%, 69.3% ± 2.2%, 83.2% ± 5.7%, 85.7% ± 3.4%, 17.8% ± 2.8%, and 14.1% ± 2.7% for the P1-3 hour, P1-6 hour, P1-18 hour, P1-24 hour, P2-3 hour, P2-6 hour, P2-18 hour, P2-24 hour, P3-3 hour, P3-6 hour, P3-18 hour, and P3-24 hour incubations, respectively; $p < .01$ between 3- or 6-hour incubation vs. 18- or 24-hour incubation at each passage). The 3- and 6-hour incubations of P4 were significantly less than those of P1 to P3 (Fig. 2A). Thus, cell growth and in vivo transplantation of GFP-transfected hMSCs were determined at 3 or 6 hours of P1 to P3.

Cell Growth of GFP-Transfected hMSCs

Initially, 2.5×10^4 of both 3-hour and 6-hour cells were counted at day 0 of the control (no transfected hMSCs) and first-, second-, and third-passage cells. Both control and first-passage cells proliferated more than three times at day 3, whereas second- and third-passage cells proliferated fewer than two times at day 3. There were significant differences between control or first-passage cells and second- or third-passage cells from day 1 to day 3 (Fig. 2B). We therefore decided to use 3- or 6-hour-incubated first-passage GFP-transfected hMSCs in vivo. All cell counting was measured in triplicate, and the average value was calculated for each plate. Cell death was minimal, and trypan blue cell viability assay revealed fewer than 3% nonviable cells up to day 3 in FBS.

Blood Flow

Tissue blood flow varied among animals. Initial blood flow at just before severance and ligation was 10–30 ml/minute per 100 g (tissue) and dropped to almost 0 just after ligation. Blood flow of each animal either 1 week or 2 weeks later was normalized to each animal's blood flow at preligation. Relative blood flow in the no-reconstruction group was 0.62 and 1.00 at 1 week and 2 weeks after experiment, respectively. There was a significant difference between 1 week and 2 weeks in the no-reconstruction group. The value in the control group with the vascularized epigastric flap for the defects demonstrated significantly increased blood flow at 1 week with a relative value of 1.71 compared with the no-reconstruction group, but there was no significant difference between 1 week and 2 weeks. Similarly, there was a significant increase in the FGF-2-treated group at 1 week with a relative value of 1.83 compared with the no-reconstruction group. The value at 2 weeks of the FGF-2-treated group was even lower, 1.78. The GFP-hMSC-treated group and GFP-hMSC- plus FGF-2-treated group were 1.59 and 1.51 at 1 week, respectively, and there was a significant increase by 2 weeks in both groups, to 2.15 and 2.29, respectively. At 2 weeks, combined GFP-hMSC and FGF-2 treatment demonstrated the most significant blood flow increase. Except for the GFP-hMSC group, there was a significant difference (1.00, 1.71, and 1.78 for no-reconstruction, control, and FGF-2 groups, respectively; $p < .01$) (Fig. 3).

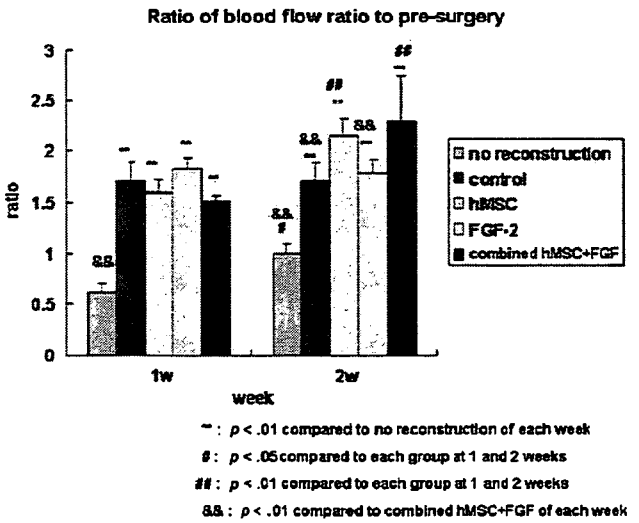

Figure 3. Tissue blood flow relative to the presurgical value. A noncontact laser blood flowmeter was used. Data samplings were repeated five times, and the mean value for each animal was adopted for further group analyses. Measurements were performed at the distal periphery of the severed and ligated femoral vessels preligation (10 animals per group), immediately after ligation (10 animals per group), at 1 w (5 animals per group), and at 2 w (5 animals per group). There was a significant blood flow increase in all group using the vascularized epigastric flap compared with the no-reconstruction group at 1 and 2 w ($p < .01$). The green fluorescent protein-hMSC and FGF-2 group demonstrated a significant time-dependent increase compared with control (flap-alone) and FGF-2-alone groups at 2 w ($p < .01$). Abbreviations: FGF, fibroblast growth factor; hMSC, human MSC; w, week(s).

Nerve Conduction Velocity

Baseline sensory maximum nerve conduction velocity (sMNCV) was obtained just before nerve severance and ligation for each animal. Presurgical sMNCV varied from 3.23 to 33.33 m/second. Once the nerve was severed, the sMNCV immediately after surgery was 0 m/second for all examined nerves. The sMNCV of each animal either 1 week or 2 weeks later was normalized to each animal's sMNCV presurgery.

The relative value of no reconstruction was 0.05 and 0.08 at 1 and 2 weeks, respectively. All groups except the control at 2 weeks demonstrated significantly improved sMNCV compared with no reconstruction (0.13, 0.14, 0.14, 0.30, 0.15, 0.21, 0.44, and 0.68 for control at 1 week, control at 2 weeks, GFP-hMSC at 1 week, GFP-hMSC at 2 weeks, FGF-2 at 1 week, FGF-2 at 2 weeks, GFP-hMSC and FGF-2 at 1 week, and GFP-hMSC and FGF-2 at 2 weeks, respectively; $p < .01$ compared with each week of no reconstruction except the 2-week control). The value of sMNCV in the GFP-hMSC group and the GFP-hMSC with FGF-2 group demonstrated a significant increase between 1 and 2 weeks after surgery (0.14 and 0.44 vs. 0.30 and 0.68 for the GFP-hMSC and GFP-hMSC with FGF-2 group at 1 week vs. the GFP-hMSC and GFP-hMSC with FGF-2 group at 2 weeks, respectively; $p < .01$) (Fig. 4).

Correlation Between Maximum Sensory Nerve Conduction Velocity and Tissue Blood Flow

The correlation between maximum sensory conduction velocity and tissue blood flow was analyzed with a simple regression curve of the independent value of all blood flow and of a dependent value of maximum nerve conduction velocity. A significant positive correlation was observed between the two with the following formula: $y = 0.22x - 0.12$; $r = 0.58$; $p < .01$.

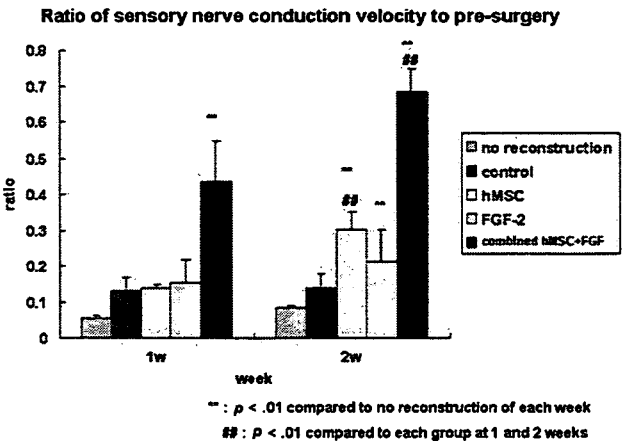

Figure 4. Sensory nerve maximum conduction velocity relative to the presurgical value. Needle electrodes were set with a 5-mm gap at the saphenous nerve after meticulous dissection from other tissues under a microscope, and all nerve experiments were shielded by a magnetic shield cage. All nerve conduction velocity data were immediately transferred to an AD converter. Data samplings were repeated five times, and the mean value for each animal was adopted for further group analyses. Measurements were performed at the distal periphery of the severed nerves and vessels preligation (10 animals per group), immediately after ligation (10 animals per group), at 1 w (5 animals per group), and at 2 w (5 animals per group). There was a significant nerve conduction velocity increase in the green fluorescent protein (GFP)-hMSC and FGF-2 group compared with other groups at 1 and 2 w ($p < .01$). The GFP-hMSC-alone and GFP-hMSC and FGF-2 groups demonstrated a significant time-dependent increase ($p < .01$). The GFP-hMSC and FGF-2 group demonstrated the most significant increase at 2 w ($p < .01$). Abbreviations: FGF, fibroblast growth factor; hMSC, human MSC; w, week(s).

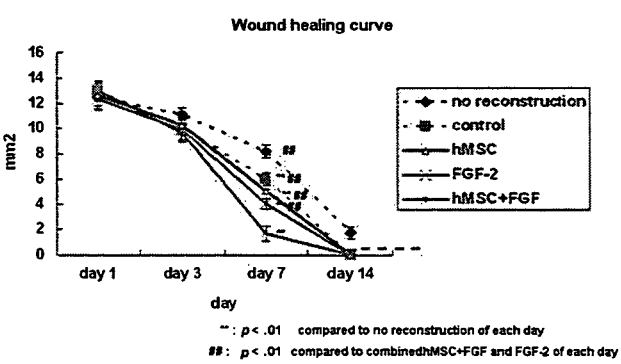

Figure 5. Wound healing curve of the ipsilateral paw. The initial wound size was 12.56 mm^2 and was measured at days 1, 3, 7, and 14. The wound size in the supine position was photographed using a 600 million dots-per-inch digital camera and an image analyzer (NIH Image, version 1.62) on a Macintosh computer. The macroscopic size of the remaining wounds was calculated three times. Significantly accelerated wound healing was observed in the green fluorescent protein-hMSC and FGF-2 group compared with any other group at day 7 ($p < .01$). All wounds except the no-reconstruction group demonstrated complete healing by day 14. Abbreviations: FGF, fibroblast growth factor; hMSC, human MSC.

Wound Healing of the Paw

The wound size was initially 12.56 mm^2 at day 0. At day 1, the mean wound size with no reconstruction, the control, GFP-hMSC, FGF-2, and GFP-hMSC and FGF-2 was 12.46, 12.95, 12.64, 12.42, and 13.00 mm^2, respectively. There was no significant difference from day 1 to day 3. The wound size was significantly smaller in the GFP-hMSC-treated wound group than any other group at day 7. Wounds in all groups but the

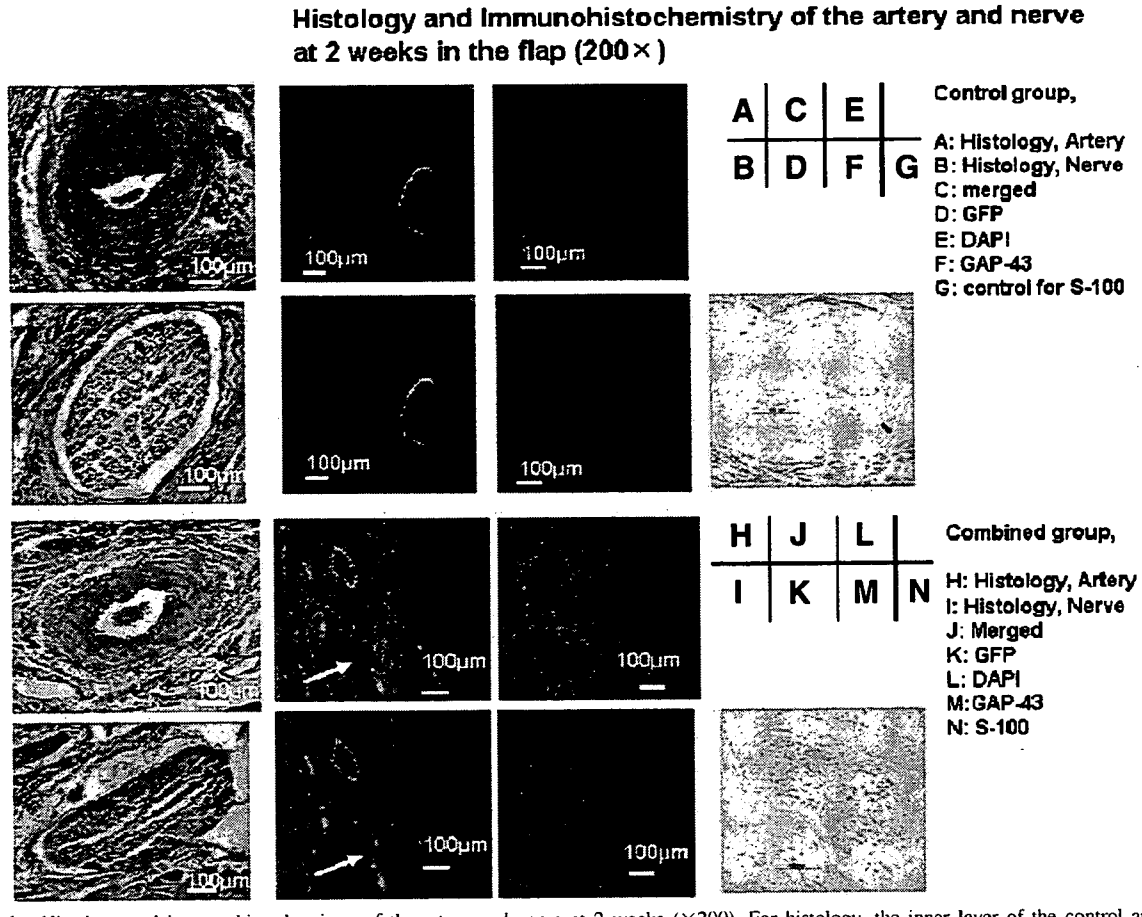

Figure 6. Histology and immunohistochemistry of the artery and nerve at 2 weeks (×200). For histology, the inner layer of the control artery was hypertrophic, and the nerve was atrophic. The control nerve was fragile and isolated from the surrounding connective and capillary tissues. Combined GFP-human MSC (hMSC)- and fibroblast growth factor-2 (FGF-2)-treated artery was more elastic, and the nerve demonstrated more dense and tight organization (**A, B, H, I**). In the control, there was no immunoreactivity of GAP-43 or traceable GFP-positive cells except the internal elastic lamina, which is considered a nonspecific immunoreaction (**C–F**). The greatest immunoreactivity of GAP-43 was seen in the GFP-hMSC- and FGF-2-treated group. More intense immunoreactivity was observed near the artery and the GFP-hMSC and FGF-2 group mainly between the artery and the nerve (**J–M**). The arrows indicate triple coexpressions of GFP, GAP-43, and DAPI. S-100 protein was diffusely expressed in the combined GFP-hMSC and FGF-2 treatment group as brown chromogen (**G, N**). Abbreviations: DAPI, 4′,6-diamidinophenylindole dihydrochloride; GFP, green fluorescent protein.

no-reconstruction group were healed by day 14. The no-reconstruction group demonstrated wounds of 1.76 mm^2 (Fig. 5).

Histology

The distal region from the severed and ligated saphenous nerve and femoral artery was histologically examined at 2 weeks postoperatively. The inner layer of the control artery was hypertrophic, and the nerve was atrophic. In contrast, the FGF-2-treated artery and nerve were more vascularized around the neuron-vascular bundles. The GFP-hMSC-treated artery was more elastic, and the nerve demonstrated denser and tight organization; the GFP-hMSC-treated artery, demonstrating well-vascularized surroundings, and the saphenous nerve were located adjacent to the artery, with a tight connection. Nerves in the vascularized epigastric fascial flap were larger than those of severed and regenerated nerves in the distal region of the severance (Fig. 6A, 6B, 6H, 6I).

Tracking of GFP-Transfected Cells and Immunofluorescent GAP-43 Expressions

Grafted GFP-transfected hMSCs were traced 2 weeks postoperatively. In the control, there was no immunoreactivity of GAP-43 or traceable GFP-positive cells except the internal elastic lamina, which is considered a nonspecific immunoreaction. There was very faint GAP-43 immunoreactivity around the nerve of the FGF-2-treated group. The intensity of both GAP-43- and GFP-positive cells increased in the GFP-hMSC-treated group. Only the outer region of the nerve adjacent to the branch of the femoral artery demonstrated both GFP and GAP-43 with DAPI expression.

The greatest immunoreactivity of GAP-43 was in the GFP-hMSC- and FGF-2-treated group. More intense immunoreactivity was observed near the artery, and GFP-hMSCs were mainly between the artery and the nerve (Fig. 6C–6F, 6J–6M). There was coexpression in the envelope area of the nerve in the fascia of the vascularized epigastric fascial flap of the GFP-hMSC and FGF-2 group (Fig. 7).

S-100 Immunohistochemistry

Combined GFP-transfected hMSCs and FGF-2 demonstrated clear and diffuse S-100 immunoreactivity in the saphenous nerve. In the control, there was no S-100 immunoreactivity in control group immunohistochemistry (Fig. 6G, 6N).

DISCUSSION

The human green fluorescent protein plasmid was successfully transfected to bone marrow-derived human mesenchymal stem

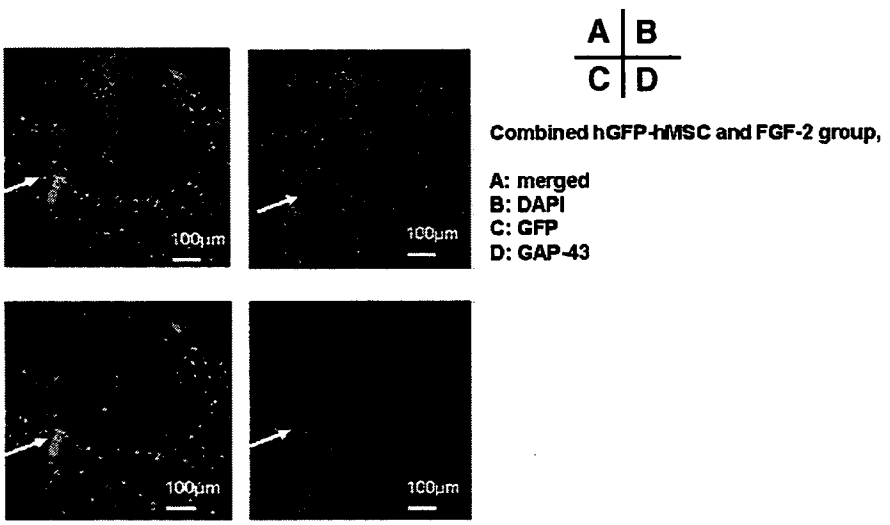

Figure 7. Immunoreactivity of GAP-43, GFP, and DAPI in control and GFP-hMSC groups at 2 weeks (×200). The outer areas of the nerve in the GFP-hMSC and FGF-2 treatment group demonstrated the coexpression of Gap-43, GFP, and DAPI. The arrows indicate triple coexpressions of GFP, GAP-43, and DAPI. Abbreviations: DAPI, 4′,6-diamidinophenylindole dihydrochloride; FGF, fibroblast growth factor; GFP, green fluorescent protein; hGFP, human green fluorescent protein; hMSC, human MSC.

cells. Transfection efficiency was conserved up to the third passage with 3- or 6-hour incubation. With 18- and 24-hour incubation, transfection efficiency significantly dropped at second and third passages compared with those with 3- and 6-hour incubation. In terms of cell proliferation, only first-passage cells demonstrated proliferation similar to that of the nontransfected control. In the next in vivo experiment, 3- or 6-hour-incubated first-passage cells were used. In the severed and ligated saphenous nerve and femoral artery, which were wrapped by a superficial epigastric vessel vascularized fascial flap as a carrier of FGF-2 and GFP-hMSC, relative blood flow was significantly increased time-dependently in the no-reconstruction group, GFP-hMSC, and GFP-hMSC and FGF-2 groups between 1 week and 2 weeks. Efficient blood flow increase was observed when the experiment was performed with GFP-hMSCs through the vascularized epigastric artery. Maximum conduction velocity of the saphenous nerve was most significantly well-recovered in GFP-hMSC and FGF-2 treatment at 1 and 2 weeks compared with any other treatment. There was almost 70% recovery to presurgical levels at 2 weeks in GFP-hMSC and FGF-2 treatment. The regenerated nerve was found at the distal site of the severed nerve. GAP-43 immunoreactivity was most clearly observed when reconstruction was performed with GFP-hMSC and FGF-2 treatment. The location of GAP-43 was mainly perineural tissues between the nerve and artery. This suggests that the bloodstream induced nerve regeneration. Nerve conduction velocity and blood flow are important, as a significant decrease of sciatic nerve blood flow and saphenous nerve conduction velocity was observed in streptozotocin-induced diabetic rats [22]. Basic fibroblast growth factor alone directly promotes the extension of regeneration of the frozen saphenous nerve in vivo [23] at 2 and 5 days. The nerve fiber regrowth demonstrated by S-100 immunohistochemistry was observed in the combined GFP-hMSC- and FGF-2-treated group, which is further evidence of this treatment efficacy in nerve regeneration [6]. In our experiments, FGF-2 enhanced tissue blood flow compared with no reconstruction at 1 and 2 weeks. The correlation between blood flow and nerve conduction velocity demonstrated a significant positive correction. The greater blood flow in the severed nerve in situ promotes better recovery of sensory nerve conduction. Blood flow is synergistically increased in the presence of GFP-hMSC at 2 weeks. This may be because FGF-2 induces blood flow not only via the arterial pedicle but by direct proliferation and differentiation effects to hMSCs, which was also observed in another wound healing model using a bilayered collagen sponge [21]. Wound healing was significantly improved with GFP-hMSC and FGF-2 treatment by 1 week. All wounds with a vascularized epigastric flap were completely healed by 2 weeks. Wounds with no reconstruction by a flap showed delayed healing at 1 and 2 weeks, and the wound was not healed by 2 weeks, whereas wounds of other groups with vascularized flap augmentation demonstrated complete healing. This investigation may contribute to human mesenchymal stem cell grafting by a vascularized epigastric flap model with cytokines leading to more local blood flow and nerve recovery, which is a fundamental factor in traumatized, diabetic, and vascular clinical settings.

ACKNOWLEDGMENTS

This study was supported by Grants 16390511, 16591795, 16659487, 16791091, 17659562, 17659563, 18390478, 18591967, and 18659526 from the Ministry of Education, Sports and Culture of Japan.

DISCLOSURE OF POTENTIAL CONFLICTS OF INTEREST

The authors indicate no potential conflicts of interest.

REFERENCES

1 Kim LR. Whelpdale K. Zurowski M et al. Sympathetic denervation impairs epidermal healing in cutaneous wounds. Wound Repair Regen 1998:6:194–201.
2 Souza BR. Cardoso JF. Amadeu TP et al. Sympathetic denervation accelerates wound contraction but delays reepithelialization in rats. Wound Repair Regen 2005:13:498–505.
3 Smith PG. Liu M. Impaired cutaneous wound healing after sensory denervation in developing rats: Effects on cell proliferation and apoptosis. Cell Tissue Res 2002:307:281–291.
4 Ruggieri MR. Braveman AS, D'Andrea L et al. Functional reinnervation of the canine bladder after spinal root transection and immediate end-on-end repair. J Neurotrauma 2006:23:1125–1136.
5 den Dunnen WF. Meek MF. Sensory nerve function and auto-mutilation after reconstruction of various gap lengths with nerve guides and autologous nerve grafts. Biomaterials 2001:22:1171–1176.

6 Marchesi C, Pluderi M, Colleoni F et al. Skin-derived stem cells transplanted into resorbable guides provide functional nerve regeneration after sciatic nerve resection. Glia 2007;55:425–438.
7 Tohill M, Mantovani C, Wiberg M et al. Rat bone marrow mesenchymal stem cells express glial markers and stimulate nerve regeneration. Neurosci Lett 2004;27:200–203.
8 Ivie TJ, Bray RC, Salo PT. Denervation impairs healing of the rabbit medial collateral ligament. J Orthop Res 2002;20:990–995.
9 Cavanagh PR, Lipsky BA, Bradbury AW et al. Treatment for diabetic foot ulcers. Lancet 2005;366:1725–1735.
10 Akagi D, Arita H, Komiyama T et al. Objective assessment of nerve injury after greater saphenous vein stripping. Eur J Vas Endovasc Surg 2007;33:625–630.
11 Jungnickel J, Haase K, Konitzer J et al. Faster nerve regeneration after sciatic nerve injury in mice over-expressing basic fibroblast growth factor. J Neurobiol 2006;66:940–948.
12 Haastert K, Lipokatic E, Fischer M et al. Differentially promoted peripheral nerve regeneration by grafted Schwann cells over-expressing difference FGF-2 isoforms. Neurobiol Dis 2006;21:138–153.
13 Pittenger MF, Mackay AM, Beck SC et al. Multilineage potential of adult human mesenchymal stem cells. Science 1999;284:143–147.
14 Bruder SP, Jaiswal N, Haynesworth SE. Growth kinetics, self-renewal, and the osteogenic potential of purified human mesenchymal stem cells during extensive subcultivation and following cryopreservation. J Cell Biochem 1997;64:278–294.
15 Akino K, Mineta T, Fukui M et al. Bone morphogenetic protein-2 regulates proliferation of human mesenchymal stem cells. Wound Repair Regen 2003;11:354–360.
16 Krampera M, Pasini A, Pizzolo G et al. Regenerative and immunomodulatory potential of mesenchymal stem cells. Curr Opin Pharmacol 2006; 6:435–441.
17 Keilhoff G, Stang F, Goihl A et al. Transdifferentiated mesenchymal stem cells as alternative therapy in supporting nerve regeneration and myelination. Cell Mol Neurobiol 2006;26:1235–1252.
18 Akita S, Fukui M, Nakagawa H et al. Cranial bone defect healing is accelerated by mesenchymal stem cells induced by coadministration of bone morphogenetic protein-2 and basic fibroblast growth factor. Wound Repair Regen 2004;12:252–259.
19 Fukui M, Akita S, Akino K. Ectopic bone formation facilitated by human mesenchymal stem cells and osteogenic cytokines via nutrient vessel injection in a nude rat model. Wound Repair Regen 2005;13: 332–340.
20 Akita S, Rashid MA, Ishihara H et al. Cytokine-dependent gp130 receptor subunit regulates rat modified axial-pattern epigastric flap. J Invest Surg 2002;15:137–151.
21 Nakagawa H, Akita S, Fukui M et al. Human mesenchymal stem cells successfully improve skin-substitute wound healing. Br J Dermatol 2005; 153:29–36.
22 Kalichman MW, Dines KC, Bobik M et al. Nerve conduction velocity, laser Doppler flow, and axonal caliber in galactose and streptozotocin diabetes. Brain Res 1998;810:130–137.
23 Fujimoto E, Mizoguchi A, Hanada K et al. Basic fibroblast growth factor promotes extension of regenerating axons of peripheral nerve. In vivo experiments using Schwann cell basal lamina tube model. J Neurocytol 1997;26:511–528.

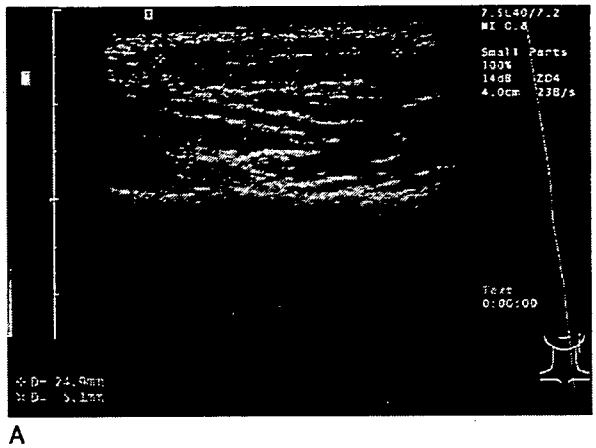

A

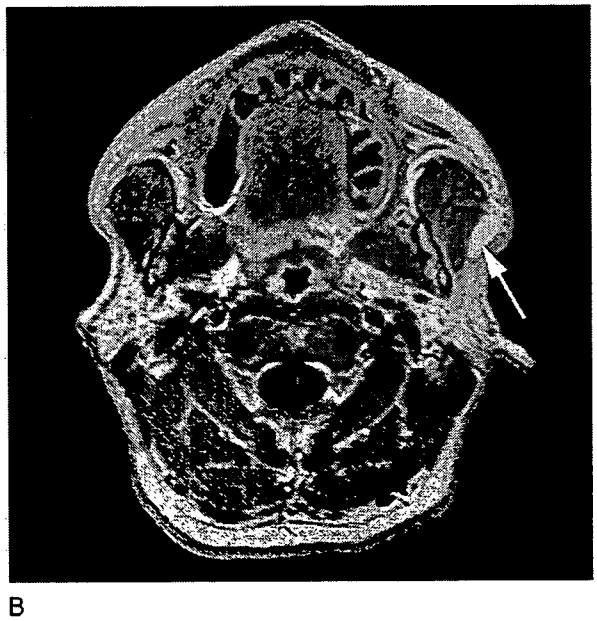

B

Fig 2 (A) Lipoma of the left parotid gland; sonographic longitudinal cross-section of the parotid region. (B) Lipoma of the left parotid gland (white arrow); axial T1-weighted, contrast-enhanced magnetic resonance image.

echoic lines with no distal enhancement or attenuation. In most cases, they have a clearly identified capsule.[3,4] The knowledge of anatomic structures and landmarks is important. According to several authors, there is a need for computed tomography or MRI to make a definite diagnosis.[5,6] A special density value or region in computed tomography is often evidence for a lipoma. The cause is usually benign in the absence of symptoms.

MRI has a high degree of intrinsic soft tissue contrast, which makes it highly suitable for imaging of salivary glands in the head and neck section.[7,8] In addition, it offers the capability to evaluate the effect of blood flow. Fatty tissue has high signal intensity on T1-weighted images and intermediate signal intensity on T2-weighted images.[9] Other masses presenting with high signal intensity are liposarcoma, hemangioma, and hemorrhage into a preexisting tumor. A liposarcoma is inhomogeneous and displays lower signal intensity than subcutaneous fat on T1-weightened sequences. In the orofacial region, liposarcomas represent a rare lesion. If there is any sign of subfascial infiltration, more attention should be given to this differential diagnosis and surgical treatment is recommended.[2,10]

References

1. Gritzmann N, Hollerweger A, Macheiner P, et al. Sonography of soft tissue masses of the neck. J Clin Ultrasound 2002;30: 356–373
2. Gaskin CM, Helms CA. Lipomas, lipoma variants, and well-differentiated liposarcomas (atypical lipomas): results of MRI evaluations of 126 consecutive fatty masses. AJR Am J Roentgenol 2004;182:733–739
3. Ahuja AT, King AD, Kew J, et al. Head and neck lipomas: sonographic appearance. AJNR Am J Neuroradiol 1998;19: 505–508
4. Zhong LP, Zhao SF, Chen GF, et al. Ultrasonographic appearance of lipoma in the oral and maxillofacial region. Oral Surg Oral Med Oral Pathol Oral Radiol Endod 2004;98: 738–740
5. Chikui T, Yonetsu K, Yoshiura K, et al. Imaging findings of lipomas in the orofacial region with CT, US, and MRI. Oral Surg Oral Med Oral Pathol Oral Radiol Endod 1997;84:88–95
6. Gritzmann N, Macheiner P. Lipoma in the parotid gland: typical US and CT morphology. Ultraschall Med 2003;24:195–196
7. Habermann CR, Cramer MC, Graessner J, et al. Functional imaging of parotid glands: diffusion-weighted echo-planar MRI before and after stimulation. Rofo 2004;176:1385–1389
8. Takashima S, Wang J, Takayama F, et al. Parotid masses: prediction of malignancy using magnetization transfer and MR imaging findings. AJR Am J Roentgenol 2001;176:1577–1584
9. Mousseaux E, Idy-Peretti I, Bittoun J, et al. MR tissue characterization of a right atrial mass: diagnosis of a lipoma. J Comput Assist Tomogr 1992;16:148–151
10. Califano L, Maremonti P, Arias GJ, et al. Infiltrating lipomas of the face. Reporting five clinical cases. An Otorrinolaringol Ibero Am 2002;29:163–172

Traumatic Unilateral Temporomandibular Joint Dislocation Overlooked for More Than Two Decades

Mitsuko Nakashima, MD, Hiroki Yano, MD, Sadanori Akita, MD, Kazuyo Tokunaga, MD, Kuniaki Anraku, MD, Katsumi Tanaka, MD, Akiyoshi Hirano, MD

Nagasaki, Japan